Component-wise approach to reinforced concrete structures

Component-Wise approach to reinforced concrete structures

Erasmo Carrera[a,b*], Riccardo Augello[a†], Alfonso Pagani[a‡], Xiangyang Xu[c§],

[a]Mul^2 Group, Department of Mechanical and Aerospace Engineering, Politecnico di Torino, 10129 Torino, Italy

[b]Department of mechanical engineering, College of engineering, Prince Mohammad Bin Fahd University P.O. Box 1664. Al Khobar 31952. Kingdom of Saudi Arabia

[c]School of rail transportation, Soochow University, Suzhou, China

Abstract: *With the rapid development of engineering constructions, especially transportation facilities, the structural models for the simulation of large-scale structures shall be eventually enhanced for predicting the complete three-dimensional stress and strain fields in reonforced concrete-made components. This paper proposes a component-wise approach for the modeling of reinforced concrete structures in which steel rebars and the concrete part are considered as two independent one-dimensional entities. Lagrange polynomials are used to express the cross-section deformations and different component-wise subdomains are joined by simply imposing displacement continuity at the chosen Lagrange points along the component boundary. The Finite Element (FE) method is applied to provide numerical solutions whereas Carrera Unified Formulation (CUF) is used to generate the related stiffness matrices in a compact and straightforward way. The classical case of homogenized beam solutions, as well as the one in which a virtual layer is associated with the steel zones, are implemented too. The three solutions are compared for a number of reinforced concrete beam problems, from single to double reinforced beam, including a T-shape cross-section. A final study considering transverse stiffeners (steel stirrups) is investigated. These stiffeners are modeled component-wise as well. Results clearly show the advantages and superiority of the component-wise FE-CUF based model to completely capture the three-dimensional strain and stress states, including shear ones, of reinforced concrete structures.*

Keywords: Component-Wise; Reinforced Concrete; One-Dimensional Model; Finite Element Model; Carrera Unified Formulation.

*Full Professor. E-mail: erasmo.carrera@polito.it
†Research Assistant. E-mail: riccardo.augello@polito.it
‡Full Professor. E-mail: alfonso.pagani@polito.it
§Full Professor. E-mail: x.y.xu@suda.edu.cn

1 Introduction

During the last decades, tall towers and long-span bridges have arisen in most of the cities around the world. This aspect was confirmed and encouraged by the rapid evolution of civil engineering, relying on always more sophisticated computer-aided techniques and complex analyses. Among the others, the Finite Element Method (FEM) represented a strong and notable tool for the growth in the knowledge of structural engineering. Due to the heterogeneous nature of the components of a RC structure (concrete and steel), nowadays approaches rely on mathematical models based on 3D elements, requiring a high effort in terms of computational cost.
In general, buildings and bridges consist of a pattern of beams and columns. Many investigations focused on modeling the mechanical behavior of Reinforced Concrete (RC) beams and columns. A comprehensive review of the argument can be reached in the work by Takizawa [1] and Umemura and Takizawa [2]. Considering that one-dimensional (1D) mathematical models are widely employed to study the structural behavior of slender bodies, they can also be applied to RC beam structures. Moreover, the simplicity of 1D theories and their wide range of applications coupled with their computational efficiency are some of the main reasons why structural engineers rely on beams rather than two-dimensional (2D) and three-dimensional (3D) heavier models. The classical and best-known beam theories consist in the Euler-Bernoulli Beam Model (EBBM) ([3, 4]) and the Timoshenko Beam Model (TBM) ([5, 6]). EBBM does not consider the transverse shear components and rotatory inertia, whereas the TBM accounts for a uniform shear distribution over the cross-section of the beam, including the effects of rotatory inertia. According to EBBM, the deformed cross-section remains plane and orthogonal to the beam axis. However, it neglects the cross-sectional shear deformation phenomena. This drawback makes the classical theories able to describe the mechanical behavior of thin and slender structures. Instead, when dealing with short beams or composite structures, the shear stresses play an important role. Then, this theory could lead to incorrect results. For this reason, the TBM represents an improved model by accounting for a uniform shear distribution.
Classical beam models yield reasonably good results when slender, solid section, homogeneous structures are subjected to bending. Nevertheless, the analysis of deep, thin-walled, open section beams requires the adoption of more sophisticated mathematical models to achieve sufficiently reliable results ([7]). For instance, one of the main issues related to TBM is that the homogeneous conditions of the transverse stress components at the top and bottom surfaces of the beam are not fulfilled. To overcome this problem, the third-order displacement field known as the Vlasov beam theory ([8]) was developed. It represents an improvement of the EBBM and TBM since the torsional moment is included within the model.
Over the last century, many refined beam theories were proposed to overcome the limitations of classical beam modeling. An exhaustive and comprehensive review on beam theories can be found in ([9, 10]). Different approaches were used to improve the beam modeling, which includes the use of warping functions based on de Saint-Venant's solution. For instance, El Fatmi and Zenzri [11] applied the de Saint-Venant's model for the analysis of composite beams. El Fatmi [12, 13] included the effects of torsion and shear forces for structures made of isotropic elastic material. A model able to deal with any arbitrary geometry of the cross-section of isotropic and anisotropic straight prismatic beams was described by Ladevèze and Simmonds [14] and by Ladevèze *et al.* [15]. The extension to free vibration analysis and composite materials was proposed by Rand [16] and Kim and White [17], respectively. Another contribution in the field of more refined 1D theories is represented by the variational

asymptotic solution (VABS). This theory allows for the analysis of a thin-walled cross-section. For example, Berdichevsky *et al.* [18] proposed the analysis of anisotropic thin-walled beams with closed sections, whereas the case of I-shape beams was investigated by Volovoi *et al.* [19]. Popescu and Hodges dealt with arbitrary cross-section and anisotropic material [20]. Another important contribution in the analysis of isotropic and prismatic beams with arbitrary cross-section was proposed by Yu *et al.*[21] and, starting from TBM, by Yu and Hodges [22, 23]. VABS application was further extended to vibration analysis of composite and thin-walled beams, see Kim and Wand [24] and Firouz-Abadi [25], respectively. For completeness reasons, the Generalized Beam Theory (GBT) [26] is also mentioned here. GBT allows for the accurate description of arbitrary thin-walled cross-section, included the circular shape. Silvestre and Camotin [27] and Silvestre [28] adopted this approach for the analysis of orthotropic materials and buckling of circular tubes, respectively. The compression case was also investigated by Bebiano [29], with non-uniform transverse loading conditions.
As a general guideline, it can be pointed out that by increasing the refinement of the kinematic field, the accuracy of the 1D model increases as well. ([30]). On the other hand, the primary drawbacks of a richer displacement field are the increase of equations to be solved and the choice of the terms to be added because this choice is generally problem-dependent. In this work, classical to higher-order 1D models are considered for the structural analysis of RC structures. The Carrera Unified Formulation (CUF) ([31]) represents the perfect tool to include any theory within the mathematical model. According to CUF, the 3D displacement field can be evaluated in a compact way as an arbitrary order expansion in terms of generic functions. The capability of handling arbitrary expansions makes CUF theories able to deal with arbitrary geometries, thin-walled shapes, and local phenomena as it was described for both static ([32, 33]) and free-vibration analyses ([34, 35]. Lagrange-like polynomials were introduced in the CUF framework ([36, 36]). In this class of models, the discretization of the displacement field over the cross-section is expressed as interpolation of Lagrange points. Investigations about the static behavior of isotropic [37] and composite structures [38] revealed the strength of Component-Wise (CW) models in dealing with open cross-sections, localized boundary conditions, and layerwise descriptions of composite structures. The present work wants to establish a unified framework to deal with RC beams. Thanks to the CW approach, steel reinforcements and concrete domain can be analyzed with independent kinematics from each other, using 1D beam FEs.
This paper is organized as follows: (i) Section 2 reports the present RC model, along with the adopted modeling approached for the cross-section approximation; (ii) then, the FEM is explained in Section 3; (iii) the main results are shown in Section 4, including single and double RC beams, single RC slab and a double RC beam with stirrups. Finally, the main conclusions are drawn.

2 Modeling approaches for reinforced concrete beams

RC components consist of a concrete structure in which steel bars are placed to increase the stiffness. Consider a double RC beam, as shown in Fig. 1. A Cartesian reference system is set so that the y axis is placed along the beam and steel bars length L. As a consequence, the cross-section of the structure lays on the x, z plane. The cross-section is then made by a concrete part (in blue) and steel rounds (in brown). Three different types of modelling approaches are adopted in this work (see Fig 2):

- Classical and homogenized beam approach;

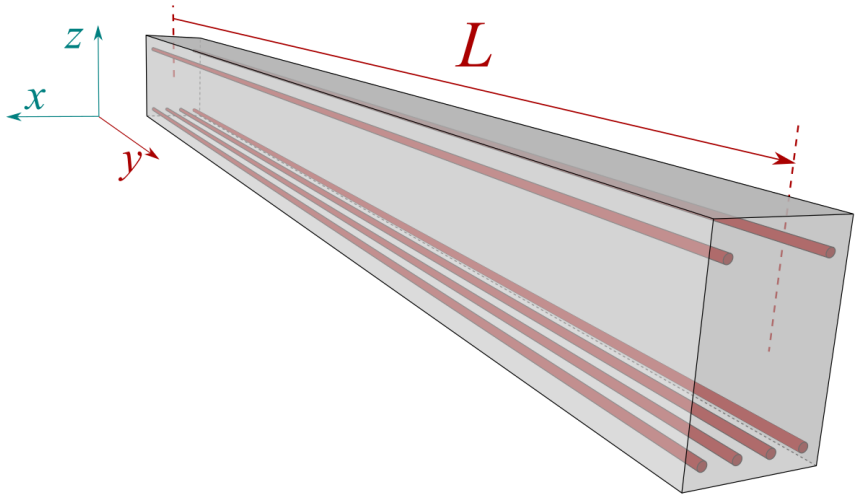

Figure 1: One-dimensional double RC structure defined over a Cartesian reference system.

- The Virtual Layer approach, here referred to as VL;
- The Component-Wise approach, here referred to as CW.

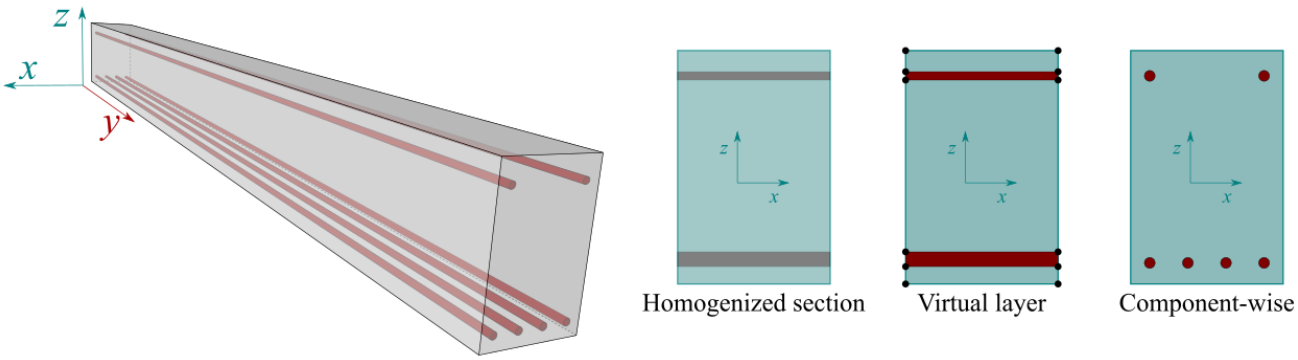

Figure 2: Beam analysis of RC structures: modeling approaches.

2.1 Homogenized section

For linear static analysis, the steel rounds can be assumed as rectangular areas A_s as described in Fig. 3, so that $A_s = \frac{k\,\pi\,\Phi^2}{4}$, where k is the number of bars and Φ is the diameter of each steel reinforcement (A_s in the tensile zone and A'_s in the compressive one). Considering an equivalent steel area for the rebars is a popular approach, see [39] for instance. In a homoge-

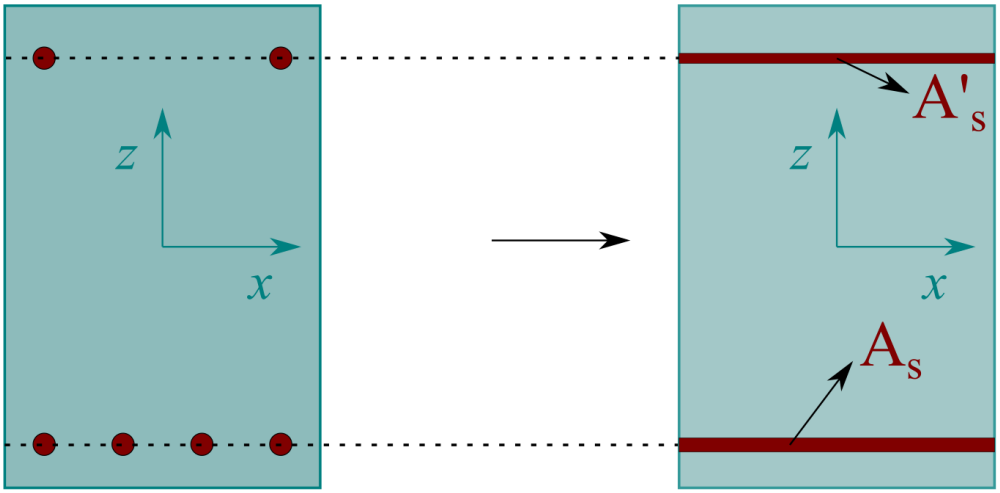

(a)

Figure 3: Steel rounds described as rectangular areas. A'_s in the compression zone, and A_s in the tension one.

nized model, a homogenization of the mechanical properties of concrete and steel is conducted by summing their contributions in the stiffness matrix. In this work, the homogenized model is employed according to Euler-Bernoulli Beam Theory (EBBM) and Timoshenko Beam Theory (TBM), as shown in 4. The 3D displacement field expressed using EBBM and TBM are

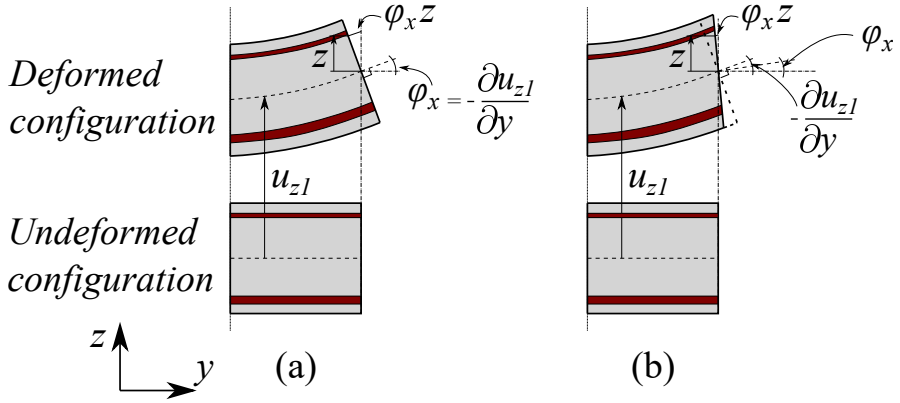

Figure 4: Schematic representation of RC beam approximated with EBBM (a) and TBM (b).

expressed in Eqs. (1) and (2), respectively.

$$\begin{aligned} u_x(x,y,z) &= u_{x_1}(y) \\ u_y(x,y,z) &= u_{y_1}(y) - \frac{\partial u_{x1}(y)}{\partial y}\,x - \frac{\partial u_{z1}(y)}{\partial y}\,z \\ u_z(x,y,z) &= u_{z_1}(y) \end{aligned} \tag{1}$$

$$\begin{array}{rcl} u_x(x,y,z) &=& u_{x_1}(y) \\ u_y(x,y,z) &=& u_{y_1}(y) \;+\; \phi_z\,(y)\;x \;+\; \phi_x\,(y)\;z \\ u_z(x,y,z) &=& u_{z_1}(y) \end{array} \tag{2}$$

where,

$$\begin{array}{rcl} \phi_z &=& \gamma_{xy} - \dfrac{\partial u_{x1}}{\partial y} \\ \phi_x &=& \gamma_{yz} - \dfrac{\partial u_{z1}}{\partial y} \\ \gamma_{xy} &=& \dfrac{\partial u_y}{\partial x} + \dfrac{\partial u_x}{\partial y} \\ \gamma_{yz} &=& \dfrac{\partial u_y}{\partial z} + \dfrac{\partial u_z}{\partial y} \end{array} \tag{3}$$

Equations (1) and (2) can be considered as a special case of the Taylor polynomial series of order 1 in the primary unknowns. It reads:

$$\begin{array}{rcl} u_x(x,y,z) &=& u_{x_1}(y) \;+\; u_{x_2}\;x \;+\; u_{x_3}\;z \\ u_y(x,y,z) &=& u_{y_1}(y) \;+\; u_{y_2}\;x \;+\; u_{y_3}\;z \\ u_z(x,y,z) &=& u_{z_1}(y) \;+\; u_{z_2}\;x \;+\; u_{z_3}\;z \end{array} \tag{4}$$

One can, then, employ Taylor polynomials of higher-order to refine the mathematical model. For instance, Eq. (5) reports the Taylor polynomial expansion series of order 2.

$$\begin{array}{rcl} u_x(x,y,z) &=& u_{x_1}(y) + u_{x_2}\;x + u_{x_3}\;z + u_{x_4}\;x^2 + u_{x_5}\;xz + u_{x_6}\;z^2 \\ u_y(x,y,z) &=& u_{y_1}(y) + u_{y_2}\;x + u_{y_3}\;z + u_{y_4}\;x^2 + u_{y_5}\;xz + u_{y_6}\;z^2 \\ u_z(x,y,z) &=& u_{z_1}(y) + u_{z_2}\;x + u_{z_3}\;z + u_{z_4}\;x^2 + u_{z_5}\;xz + u_{z_6}\;z^2 \end{array} \tag{5}$$

Classical theories, as well as Taylor polynomial expansions, are employed for the numerical results in this paper. Finally, the homogenized cross-section is shown in Fig. 5.

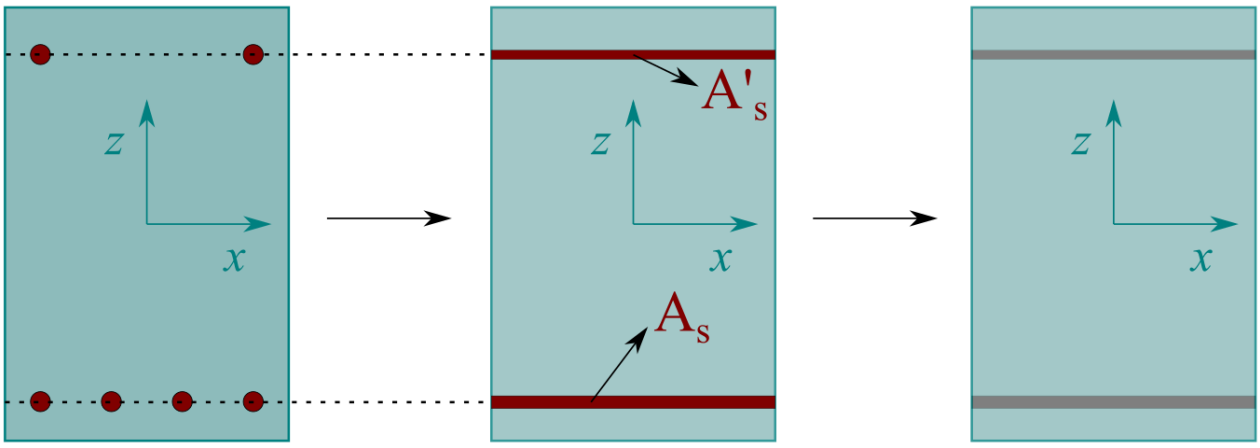

Figure 5: Homogenized assembling scheme for a RC structure.

2.2 VL models

A beam model can be imposed for each concrete and steel rebars zone. In the case of a double RC beam structure, five 1D classical models can be employed within the structure, as shown in Fig. 6. A problem arises when the compatibility condition of the displacement has to be imposed between the interfaces of each 1D beam. This issue can be mitigated employing mathematical artifices, such as the Lagrange multipliers, as shown in Fig. 6 and in Eq. (6), where Π is the contribution added to the energy of the system for the derivation of the equilibrium, λ is the vector of the Lagrange multipliers and k is the interface between the i^{th} and the $i^{th}+1$ 1D beam.

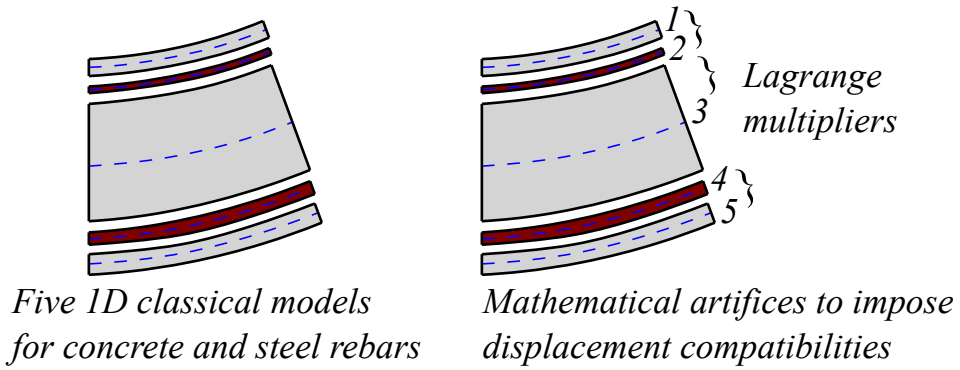

Figure 6: Displacement compatibility condition for classical 1D models.

$$\begin{aligned} \Pi &= \boldsymbol{\lambda}^T(\mathbf{u}^i(x_k,y_k,z_k) - \mathbf{u}^{i+1}(x_k,y_k,z_k)) \\ \boldsymbol{\lambda} &= \{\lambda_x,\lambda_y,\lambda_z\}^T \end{aligned} \tag{6}$$

The usage of complicated mathematical tools can be overcome by using Lagrange polynomials for expanding the displacement field. They allow the users for the employment of Lagrange Points (LPs), where displacement variables are located. In this way, by imposing LPs on the interfaces between concrete and steel rebars, the displacement compatibility is automatically ensured. An application of this method is reported in Fig. 7. The cross-section is approximated with a pattern of Lagrange Points (LPs), which are divided into opportune Lagrange polynomials. The 3D displacement field is, then, a result of an interpolation of the displacements calculated at the LPs. The degree of the interpolation is defined by the number of the employed LPs, namely a 4 LPs (L4) ensures a bilinear interpolation, a 9 LPs (L9) a quadratic interpolation and a 16 LPs (L16) a cubic interpolation. The number of DOFs equals the sum of the displacements for each LP. For an L9, as shown in Fig. 8, the interpolation functions are:

$$\begin{aligned} L_\tau &= \frac{1}{4}(r^2+rr_\tau)(s^2+ss_\tau) && \tau=1,3,5,7 \\ L_\tau &= \frac{1}{2}s_\tau^2(s^2-ss_\tau)(1-r^2)+\frac{1}{2}r_\tau^2(r^2-rr_\tau)(1-s^2) && \tau=2,4,6,8 \\ L_\tau &= (1-r^2)(1-s^2) && \tau=9 \end{aligned} \tag{7}$$

where r and s vary from -1 to $+1$, whereas r_τ and s_τ are the coordinates of the nine LPs whose locations in the natural coordinate frame are shown in Fig. 8. The relation between the natural and physical coordinates can be found in many books, see [40] for instance. Briefly,

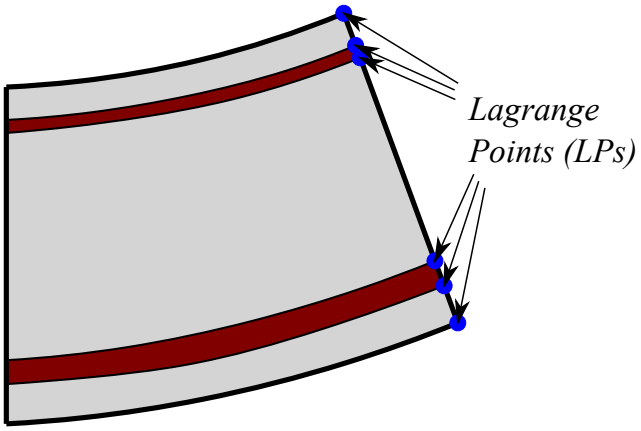

Figure 7: Displacement compatibility condition for refined 1D models with Lagrange points. The displacement compatibility is ensured "a priori" by the use of displacement values at Lagrange points as unknown variable. The Lagrange points are chosen at the interface of the various components/layers.

one can write:

$$\begin{array}{rclcccccl} x & = & L_1 x_1 & + & L_2 x_2 & + & \ldots & + & L_9 x_9 \\ z & = & L_1 z_1 & + & L_2 z_2 & + & \ldots & + & L_9 z_9 \end{array} \tag{8}$$

where $x_1, x_2, \ldots, x_9$ and $z_1, z_2, \ldots, z_9$ are the physical coordinates of the Lagrange nodes. The displacement field of a L9 is therefore

$$\begin{array}{rclcccccl} u_x(x,y,z) & = & L_1(x,z)u_{x_1}(y) & + & L_2(x,z)u_{x_2}(y) & + & \ldots & + & L_9(x,z)u_{x_9}(y) \\ u_y(x,y,z) & = & L_1(x,z)u_{y_1}(y) & + & L_2(x,z)u_{y_2}(y) & + & \ldots & + & L_9(x,z)u_{y_9}(y) \\ u_z(x,y,z) & = & L_1(x,z)u_{z_1}(y) & + & L_2(x,z)u_{z_2}(y) & + & \ldots & + & L_9(x,z)u_{z_9}(y) \end{array} \tag{9}$$

In which u_{x_1}, ..., u_{z_9} are the displacement variables of the problem and they represent the displacement components of each of the nine LPs (see Fig. 8). This approach allows for

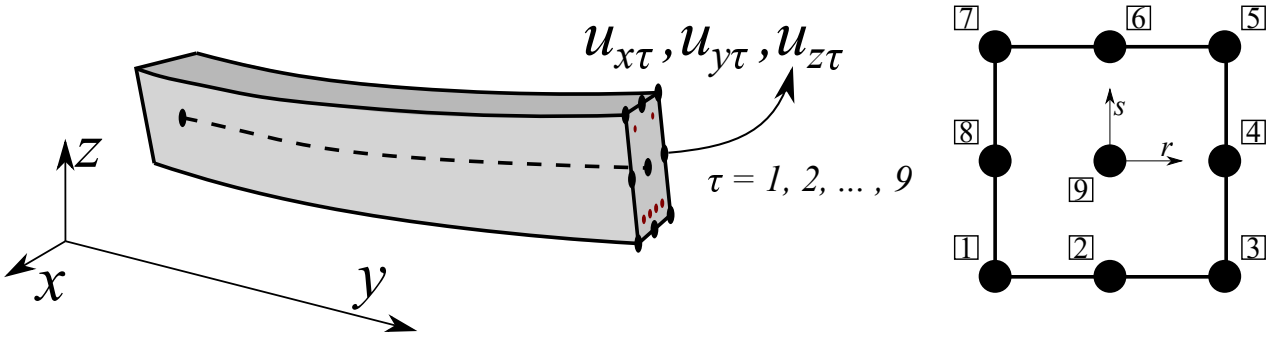

Figure 8: RC beam discreized with Lagrange points.

the imposition of LPs to subdivide the concrete and steel zones, as shown in Fig. 9. This approach is here recalled as Virtual Layer (VL), for the similar approach used for composite materials ([41]). Namely, VL considers different sets of variables per each zone (concrete and steel), and the homogenization is just conducted at the interface level, as shown in Fig. 9, where LPs are put in the interfaces between concrete and steel.

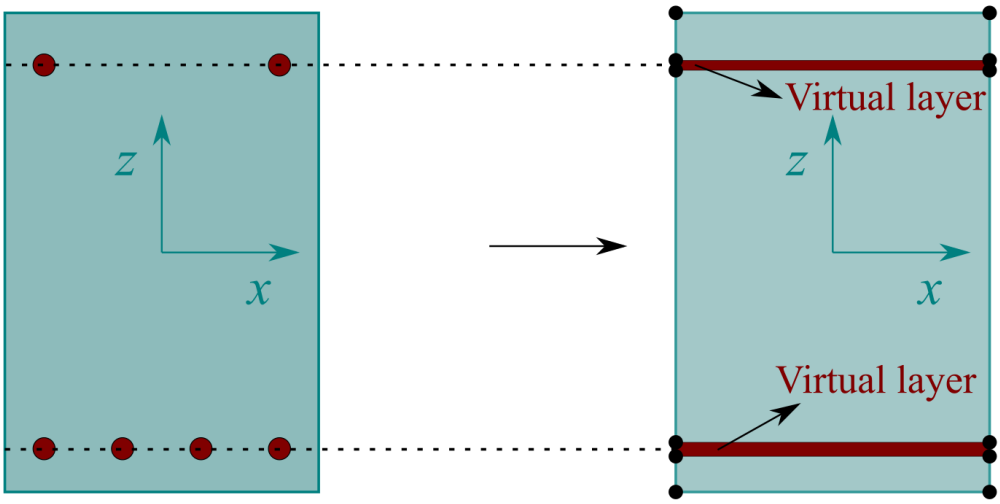

Figure 9: Virtual layer assembling scheme for a RC structure.

2.3 Component-Wise approach

As a further step, the capability of Lagrange polynomials to opportunely put LPs within the cross-section allows for the modeling of steel rebars and concrete in an independent way. Figure 10 describes the Component-Wise (CW) technique for a RC beam, whose components are modeled individually and simultaneously using LE cross-sectional elements. Each component keeps its independent material and geometrical properties. In the case of the RC components considered in the present study, LPs are employed for each component (steel and concrete), as depicted in Fig. 10. After considering the RC structure (Fig. 10(a)), the steel and the concrete components are dealt as independent entities from each other (Fig. 10(b)). Then, LPs are opportunely chosen in the boundaries of the two components (Fig. 10(c)). Finally, the components can be joined in correspondence of the aforementioned LPs (Fig. 10(d)). The resulting approach is declared as CW since multiple LPs were used to evaluate displacement variables in each structural component. This methodology allows for the tuning of the capabilities of the model by (1) choosing which component requires a more refined model and (2) setting the order of the structural model to be used. Up to now, this result could only be obtained using solid FEs. An example of CW approach can be found in [42].

2.4 Homogenized, virtual layer and component-wise approaches in a unified form

The three described approaches can be written in a unified form, recalling the Carrera Unified Formulation (CUF). Namely, according to the CUF, the 3D displacement field, as well as its variation (denoted by δ), of the structure can be written in the following unified way:

$$\begin{aligned} \mathbf{u}(x,y,z) &= F_\tau(x,z)\mathbf{u}_\tau(y), \qquad \tau = 1,2,....,M \\ \delta\mathbf{u}(x,y,z) &= F_s(x,z)\delta\mathbf{u}_s(y), \qquad s = 1,2,....,M \end{aligned} \tag{10}$$

where $\mathbf{u}(x,y,z)$ is the displacement vector, whose components are expressed in the general reference system (x,y,z) of Fig. 1, F_τ represent the cross-sectional functions depending on the x,z coordinate, τ is the sum index and M is the number of terms of the expansion in the cross-section plane assumed for the displacements. For the homogenized section approach,

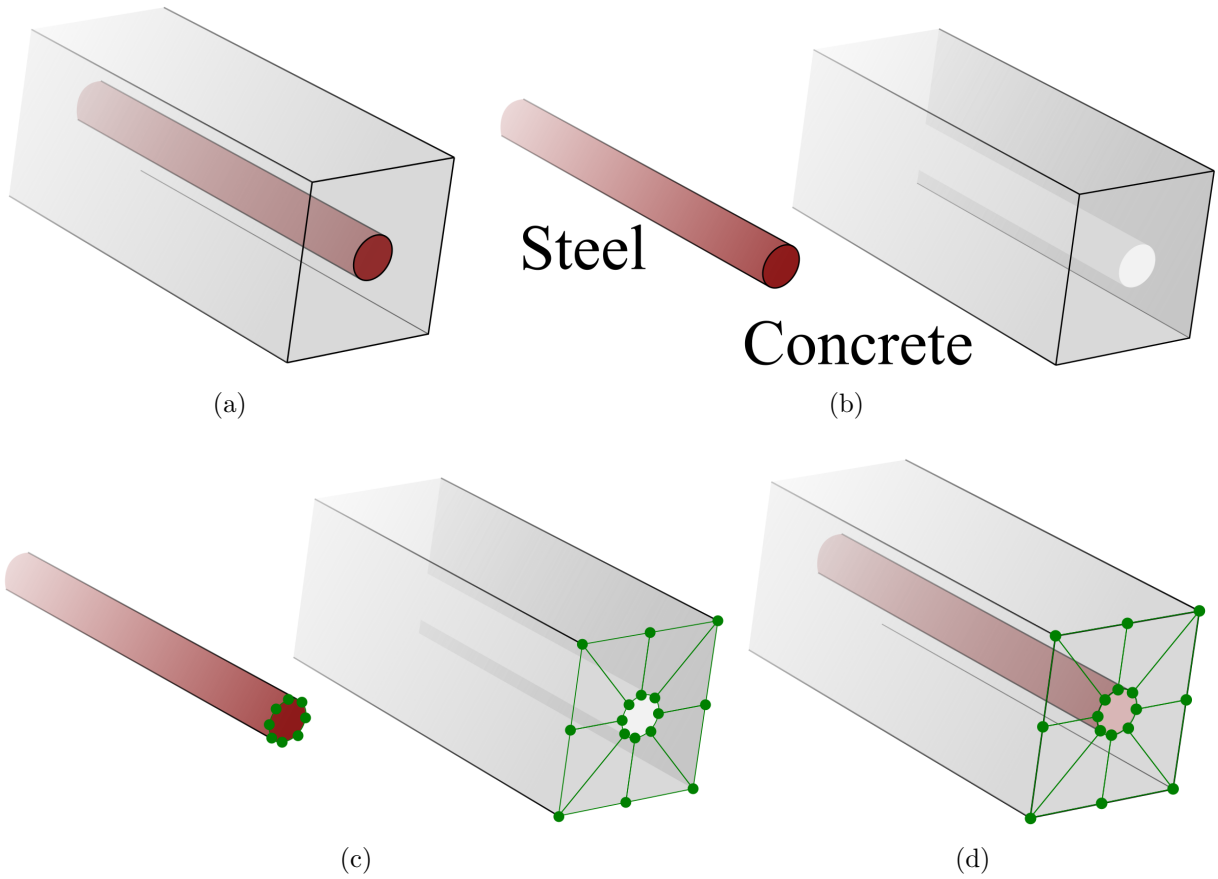

Figure 10: Component-wise approach for the cross-section discretization of a single RC beam. (a) Definition of RC structure; (b) individual definition of steel and concrete; (c) Lagrange points applied to each component boundary; (d) joining of the different components.

the classical EBBM and TBM theories are employed by using Taylor polynomials as F_τ, with no more than constant and linear terms. In case of EBBM, it becomes:

$$\begin{array}{rcl} u_x(x,y,z) &=& u_{x_1}(y)\ F_{1x} \\ u_y(x,y,z) &=& u_{y_1}(y)\ F_{1y} \ + \ \dfrac{\partial u_{x1}(y)}{\partial y}\ F_{2y} \ + \ \dfrac{\partial u_{z1}(y)}{\partial y}\ F_{3y} \\ u_z(x,y,z) &=& u_{z_1}(y)\ F_{1z} \end{array} \tag{11}$$

where $F_{1x} = F_{1y} = F_{1z} = 1$, $F_{2y} = -x$ and $F_{3y} = -z$. In the case of TBM, one has:

$$\begin{array}{rcl} u_x(x,y,z) &=& u_{x_1}(y)\ F_{1x} \\ u_y(x,y,z) &=& u_{y_1}(y)\ F_{1y} \ + \ \phi_z\ (y)\ F_{2y} \ + \ \phi_x\ (y)\ F_{3y} \\ u_z(x,y,z) &=& u_{z_1}(y)\ F_{1z} \end{array} \tag{12}$$

where $F_{1x} = F_{1y} = F_{1z} = 1$, $F_{2y} = x$ and $F_{3y} = z$. When dealing with the VL approach, the 3D displacement of a L9 can be written, in the context of CUF, as:

$$\begin{array}{rcccccccc} u_x(x,y,z) &=& F_1(x,z)u_{x_1}(y) &+& F_2(x,z)u_{x_2}(y) &+& \ldots &+& F_9(x,z)u_{x_9}(y) \\ u_y(x,y,z) &=& F_1(x,z)u_{y_1}(y) &+& F_2(x,z)u_{y_2}(y) &+& \ldots &+& F_9(x,z)u_{y_9}(y) \\ u_z(x,y,z) &=& F_1(x,z)u_{z_1}(y) &+& F_2(x,z)u_{z_2}(y) &+& \ldots &+& F_9(x,z)u_{z_9}(y) \end{array} \tag{13}$$

where the F_1, F_2, ..., F_9 are those shown in Eq. (7), when ezpressed in the physical domain. Finally, every approach here described can be written in a generic form as shown in Eq. (10).

3 Finite Element Approximation

The Finite Element Method (FEM) is adopted to discretize the structure along the y axis. Thus, the generalized displacement vector $\mathbf{u}_s(y)$ and its variation is approximated as follows:

$$\begin{array}{ll} \mathbf{u}_\tau(y) = N_i(y)\mathbf{q}_{\tau i} & i = 1, 2, \ldots, N_n \\ \delta\mathbf{u}_s(y) = N_j(y)\delta\mathbf{q}_{sj} & j = 1, 2, \ldots, N_n \end{array} \tag{14}$$

where $N_i(y)$ stands for the i-th 1D shape function, $\mathbf{q}_{\tau i}$ is the vector of the FE nodal parameters, i indicates summation and N_n is the number of the FE nodes per element. An exhaustive review of the shape functions N_i is given by Bathe [43] and by Carrera *et al.* [40, 44]. In this work, a cubic interpolation is assumed. Basically, four nodes FEs (B4) are employed to discretize the 1D structure along the y axis

3.1 Constitutive and geometrical relations

The 3D stress, $\boldsymbol{\sigma}$, and strain, $\boldsymbol{\epsilon}$, components are introduced in the following, with a vectorial notation:

$$\boldsymbol{\sigma} = \left\{ \begin{array}{cccccc} \sigma_{xx} & \sigma_{yy} & \sigma_{zz} & \sigma_{xz} & \sigma_{yz} & \sigma_{xy} \end{array} \right\}^T, \quad \boldsymbol{\epsilon} = \left\{ \begin{array}{cccccc} \epsilon_{xx} & \epsilon_{yy} & \epsilon_{zz} & \epsilon_{xz} & \epsilon_{yz} & \epsilon_{xy} \end{array} \right\}^T \tag{15}$$

Thus, the geometrical relations take the following form:

$$\boldsymbol{\epsilon} \ = \ \mathbf{b}\mathbf{u} \tag{16}$$

where $\mathbf{b}$ is the matrix of the differential operators. Interested readers can find the expression of $\mathbf{b}$ in [44, 40].

A linear elastic isotropic material is considered in this work. Consequently, the constitutive relation reads as:

$$\boldsymbol{\sigma} = \mathbf{C}\boldsymbol{\epsilon}, \tag{17}$$

where and $\mathbf{C}$ is the material elastic matrix of homogenoeus and isotropic materials. The components of $\mathbf{C}$ matrix are function of the Young modulus E and Poisson's ratio ν. If not otherwise stated, for steel reinforcements $E_s = 210$ MPa and $\nu_s = 0.3$ are assumed, whereas for concrete portion the assumed Young modulus is $E_c = E_s/n$, where n is the homogenization coefficient, taken as 15 and $\nu_c = 0.2$.

3.2 Fundamental nuclei

The principle of virtual work is recalled for the evaluation of the equilibrium equations. In the case of static analysis, it states that the virtual variation of the internal work equals the virtual variation of the external one. The formes can be expressed as follows:

$$\delta L_{\text{int}} = \int_{\Omega_k}\int_{L} \left(\delta\boldsymbol{\epsilon}^T\boldsymbol{\sigma}\right)\, \mathrm{d}\Omega_k \mathrm{d}l \tag{18}$$

where Ω_k and L are the integration domains in the cross-section and axis direction, respectively. On the other hand, from the virtual variation of the external work, the external loadings arise. Considering the constitutive equations, the geometrical relations and applying CUF and the FEM approximation, the governing equations can be obtained straightforwardly. A detailed step-by-step explanation of this procedure is described in [31]. In a compact form, the following system of linear algebraic equations holds:

$$\delta\mathbf{q}_{sj}^T\, \mathbf{K}^{ij\tau s}\, \mathbf{q}_{\tau i} = \mathbf{P}_{sj} \tag{19}$$

where $\mathbf{K}^{ij\tau s}$ is a 3×3 matrix representing the called fundamental nucleus of the mechanical stiffness matrix. The nucleus is the basic building block from which the stiffness matrix of the whole structure can be computed automatically. First, the fundamental nucleus is expanded on the indexes τ and s. Then, the matrix is assembled at the cross-sectional level depending on the considered approach. $\mathbf{P}_{sj}$ is a 3×1 matrix which consists in the fundamental nucleus of the external load. The explicit expressions of the CUF fundamental nuclei for beam structures are not reported here. Complete formulation and related mathematical passages can be found in the recent book by Carrera et al. [40]. In this paper, the main attention is focused on the use of these hierarchical nuclei for the formulation of various kinematics models with combined homogenization and VL capabilities for the cross-section domain.

4 Numerical results

In this section, the proposed FE model for the static analysis of RC structures is validate with analytical results. The following reference problems were considered to serve the scope:

- Single RC beam;
- Double RC beam;
- Single RC slab;
- Double RC beam with stirrups.

Homogenized models is here denoted as "hTN" or "hLN", where "h" stands for homogenization, T stands for Taylor expansions, L stands for Lagrange polynomials, and N denotes the number of terms of the expansion and the polynomial order.

4.1 Single reinforced concrete beam

The first analysis case regards a RC beam, as shown in Fig. 11. The length L of the beam equals 6096 mm, whereas the heigth h is equal to 543 mm and the width b measures 495 mm. The homogenization coefficient n is equal to 15, and the Young modulus of the steel E_s is equal to 210 GPa (consequently, the Young Modulus of the concrete equals $E_c = \frac{E_s}{n}$). Figure 12 depicts the cross-section of the beam. Four steel bars (diameter $\Phi = 25.4$ mm) are

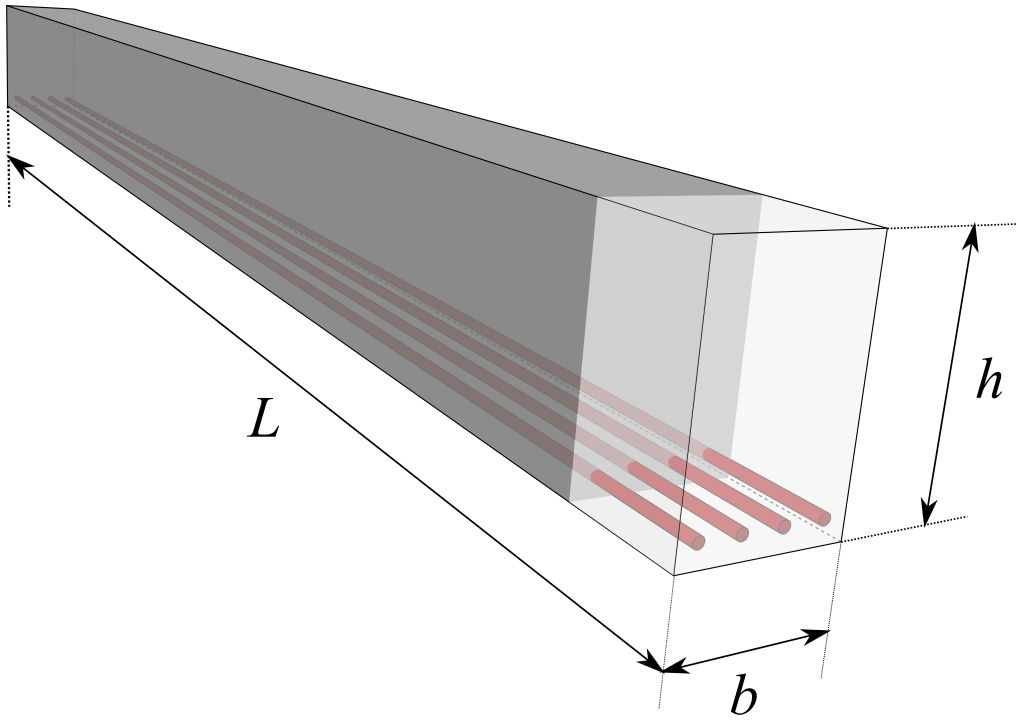

Figure 11: Geometry of the single RC beam.

equispaced and placed at a distance $d = 495$ mm from the top. For the following analysis, the four steel bars are modeled as a rectangular with area $A_s = 4\pi\Phi^2$ and placed at the same distance d than the four steel bars.
The beam is supposed to be simply supported and loaded with a uniform transverse pressure of 0.05 MPa. A preliminary convergende study was conducted to evaluate the FE model to be used. The results are shown in Fig. 13, and 20B4 FEs are chosen as converged approzimation.

Table 1 shows the vertical displacement of point $(0,\frac{L}{2},0)$ using the analytical solution and the proposed low- to higher-order beam model. Moreover, the axial stress component of concrete and steel are evaluated. The results are demonstrated to be in agreement with the analytical ones, and they increase as the refinement of the theory increases. The analytical model makes use of EBBM, considering an homogenized model.
The through-the-thickness distribution of the axial stress in the midspan of the beam is reported in Fig. 14 for every adopted kinematic order. On the other hand, Fig. 15 shows

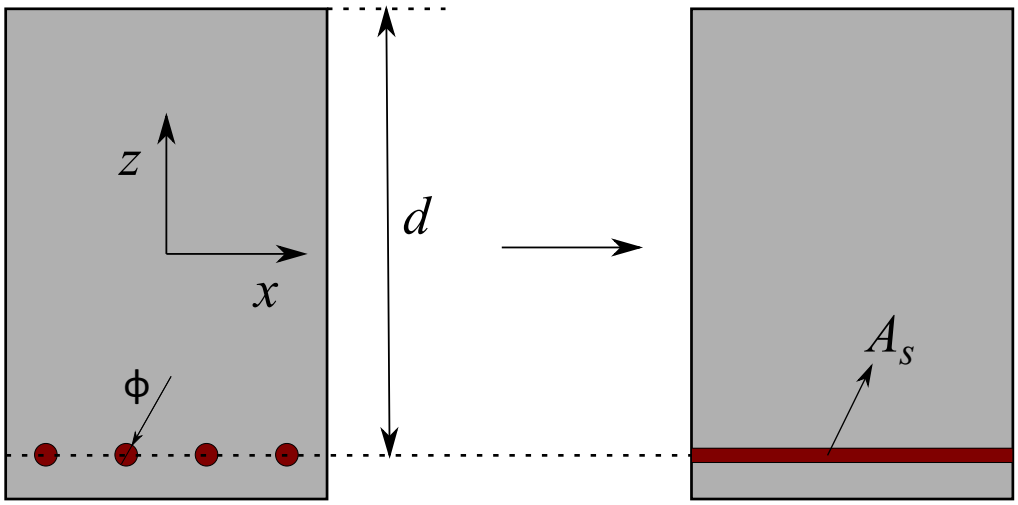

Figure 12: Cross-section geometry of the single RC beam (left) and the current cross-section (rigth).

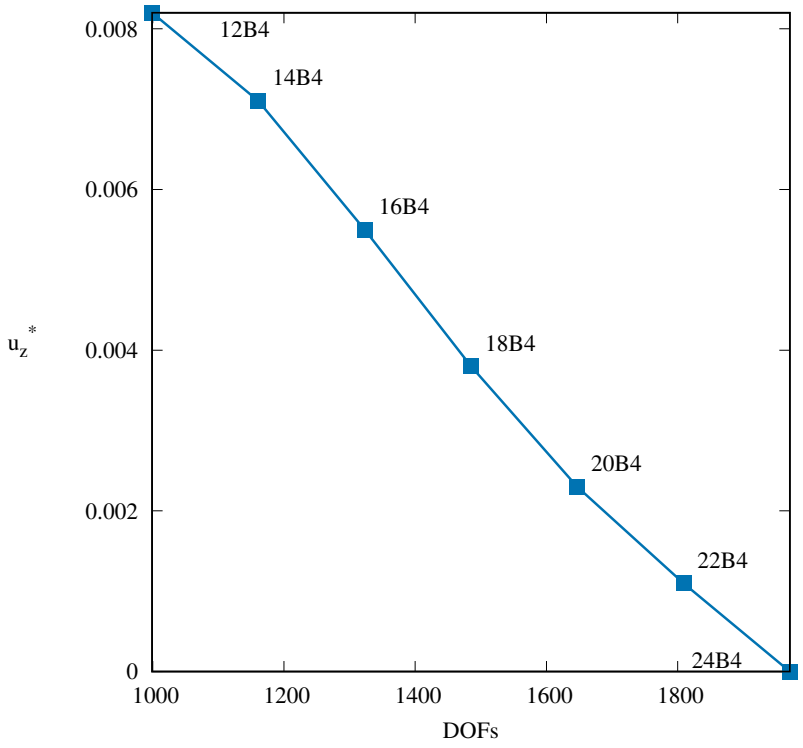

Figure 13: Convergence results for the single RC beam.

Model	$-u_z$, mm at point $(0,\frac{L}{2},0)$	$-\sigma_{yy,c}$, MPa at $\frac{L}{2}$	$\sigma_{yy,s}$, MPa at $\frac{L}{2}$	DOFs
Analytical [39]	3.8216	4.1477	40.4084	-
EBBM	3.8403	4.1571	40.3248	183
TBM	3.8997	4.1530	40.3015	305
hT1	3.8997	4.1530	40.3015	549
hT5	3.8650	4.1017	43.3864	1098
hT10	3.8841	4.1682	42.9542	1830
hL4	3.6428	4.0871	44.5910	732
hL9	3.9014	4.1362	43.0510	1647
hL16	3.9373	4.1607	42.9603	2928
VL4	3.7908	4.1763	40.5529	1464
VL9	3.9125	4.1641	41.5236	3843
VL16	3.9207	4.1506	41.5813	7320

Table 1: Values of the transverse displacement of point $(0,\frac{L}{2},0)$ and axial concrete and steel stress of a simply supported RC beam undergoing a vertical uniform pressure. Analytical solution compared to the homogenized and VL models of Fig. 12.

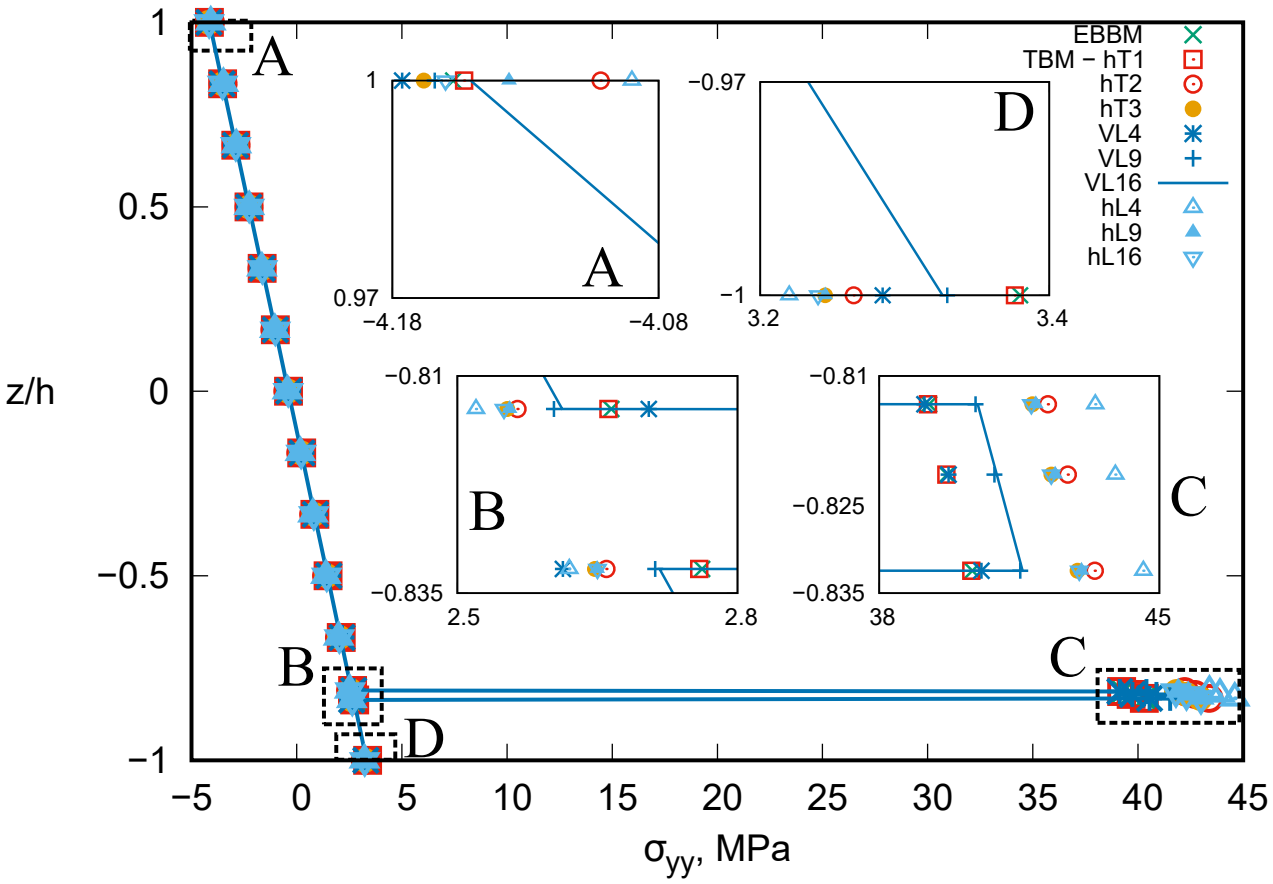

Figure 14: Through-the-thickness σ_{yy} distribution for the single RC beam at $y = \frac{L}{2}$.

the σ_{yz} for every theory, along with a focus on the L16 model. To address the capability of the present mathematical approach, three aditional schematic representation of the single RC beam is considered. They are described in Fig. 16 and, in particular, the CW approach is used for Fig. 16(c). The results for the Fig. 16(a) model are reported in Table 2, and they show a great accuracy compared to the previous approach. The through-the-thickness

Model	$-u_z$, mm at point $(0,\frac{L}{2},0)$	$-\sigma_{yy,c}$, MPa at $\frac{L}{2}$	$\sigma_{yy,s}$, MPa at $\frac{L}{2}$	DOFs
Analytical [39]	3.8216	4.1477	40.4084	-
EBBM	3.8429	4.1601	39.8444	183
TBM	3.9022	4.1559	39.8287	305
hT1	3.9022	4.1559	39.8287	549
hT5	3.8677	4.1049	42.8737	1098
hT10	3.8871	4.1779	42.3277	1830
hL4	3.6829	4.0925	43.8462	1464
hL9	3.8839	4.1385	42.2806	3843
hL16	3.9064	4.1609	42.1581	7320
VL4	3.8971	4.1817	39.9277	2928
VL9	3.9302	4.1676	40.9402	8967
VL16	3.9334	4.1538	40.9922	18300

Table 2: Values of the transverse displacement of point $(0,\frac{L}{2},0)$ and axial concrete and steel stress of a simply supported RC beam undergoing a vertical uniform pressure. Analytical solution compared to the homogenized and VL models of Fig. 16(a).

σ_{yy} and σ_{yz} distributions are reported in Fig. 17. Moreover, the results for the Fig. 16(b) model are described in Table 3, and they show a great accuracy compared to the previous approaches. The through-the-thickness σ_{yy} and σ_{yz} distributions are reported in Figs. 18 and 19. The capability of the present approach to accurately describe the through-the-thickness stress distribution is ensured, whether if the steel is excluded or included. The CW approach, described in Fig. 16(c), is adopted to analyze the reinforcement bars with a own independent kinematic from the concrete zone. L16 elements are used for the cross-section discretization, with 206058 DOFs. The results are described in Table 4, and the distributions of the through-the-thickness σ_{yy} and σ_{yz} are reported in Figs. 20 and 21 Finally, configurations of the CW approach for the σ_{yz} and σ_{yz} distributions are reported in Fig. 22.

4.2 Double RC beam

As a further analysis, a double RC beam is considered. The geometry is shown in Fig. 23, where L = 8555.8 mm, b = 406 mm and h = 762 mm. The cross-sectional geometric properties are reported in Fig. 24. 2 steel bars are used in the compression zone, whereas 8 bars in the tension one, with Φ = 25.4 mm. Finally, d = 660 mm and d' = 64 mm. The structure is analyzed using the LW approach, so that the bars are simulated with an equivalent portion with the same area, so that $A'_s = 1290$ mm^2 and $A_s = 5161$ mm^2.
In this context, preliminary convergence analysis is performed and the results are shown in Fig. 25. Clearly, a 20 B4 configuration can be considered as reliable and, therefore, is used for the subsequent analysis as axial discretization. Then, the static analysis is performed. The

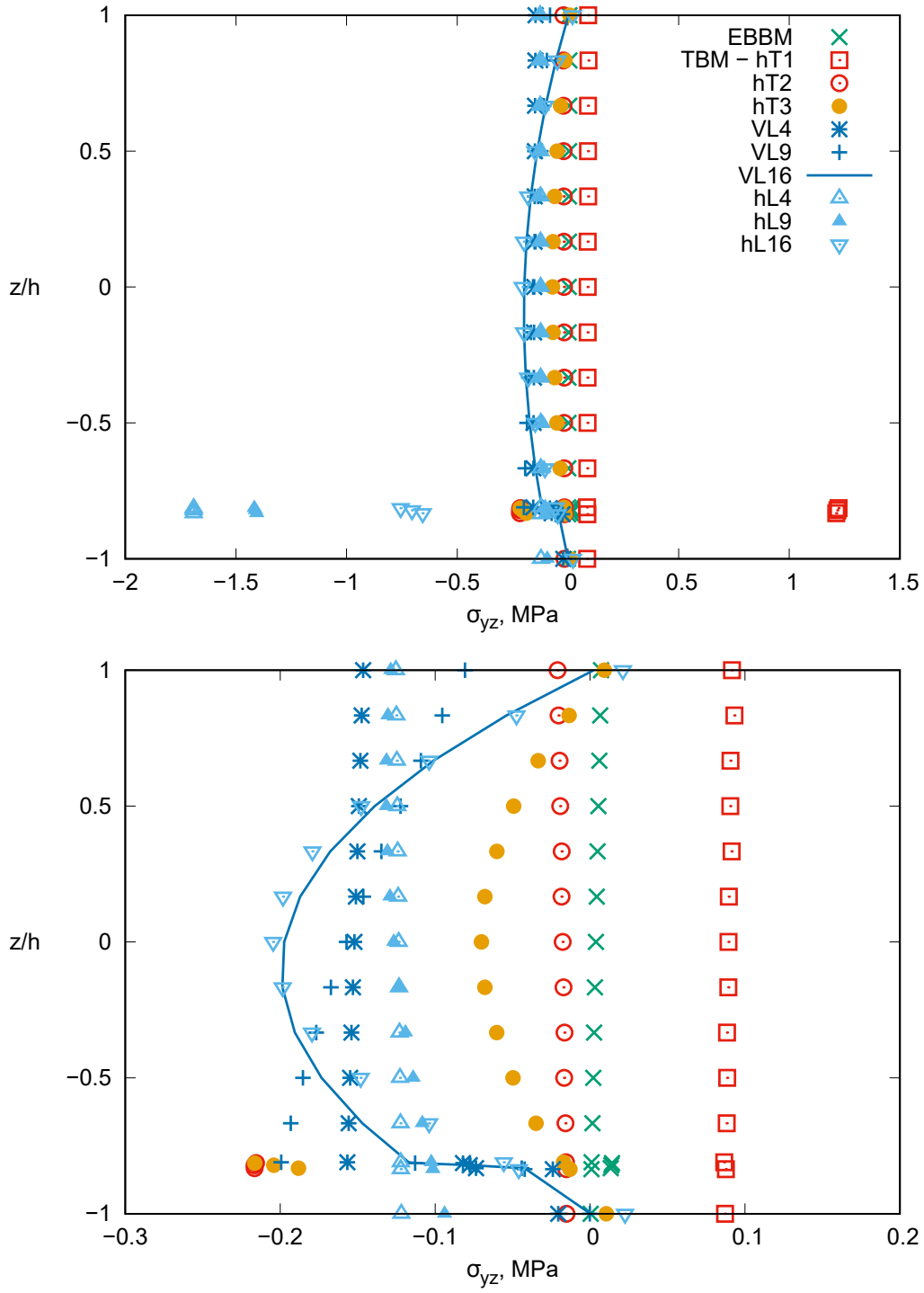

Figure 15: Through-the-thickness σ_{yz} distribution for the single RC beam at $y = \dfrac{L}{2}$.

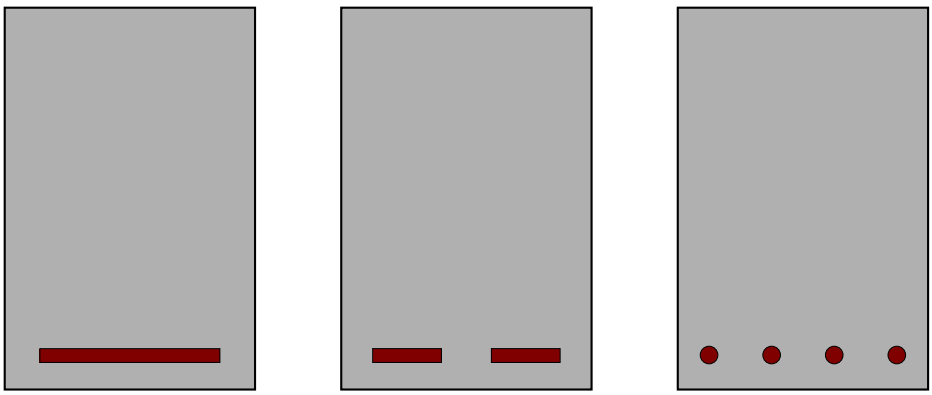

(a) (b) (c)

Figure 16: Different cross-section approximation for the single RC beam.

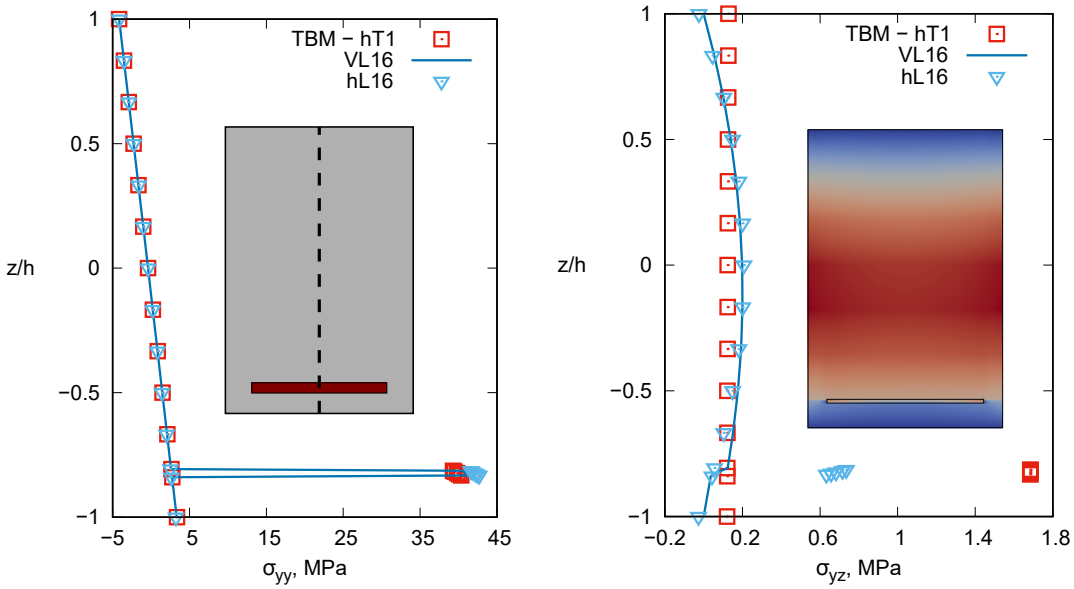

Figure 17: Through-the-thickness σ_{yy} and σ_{yz} distributions for the single RC beam at $y = \dfrac{L}{2}$ for the cross-section approximation 16(a).

Model	$-u_z$, mm at point $(0,\frac{L}{2},0)$	$-\sigma_{yy,c}$, MPa at $\frac{L}{2}$	$\sigma_{yy,s}$, MPa at $\frac{L}{2}$	DOFs
Analytical [39]	3.8216	4.1477	40.4084	-
EBBM	3.8387	4.1588	39.8033	183
TBM	3.8982	4.1545	39.7877	305
hT1	3.8982	4.1545	39.7877	549
hT5	3.8606	4.1034	42.8291	1098
hT10	3.8802	4.1704	42.4546	1830
hL4	3.7054	4.0858	43.3656	2196
hL9	3.8749	4.1388	42.0996	6039
hL16	3.9043	4.1591	41.8769	11712
VL4	3.9062	4.1765	39.8295	4392
VL9	3.9106	4.1673	40.7289	14091
VL16	3.9186	4.1458	40.7551	29280

Table 3: Values of the transverse displacement of point $(0,\frac{L}{2},0)$ and axial concrete and steel stress of a simply supported RC beam undergoing a vertical uniform pressure. Analytical solution compared to the homogenized and VL models of Fig. 16(b).

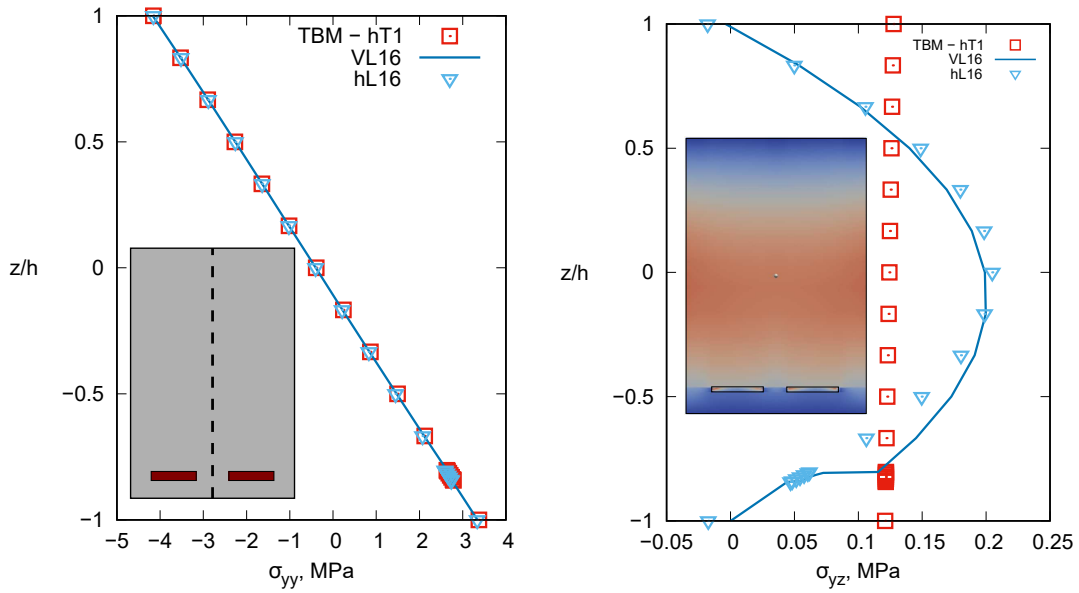

Figure 18: Through-the-thickness σ_{yy} and σ_{yz} distribution for the single RC beam at $y = \frac{L}{2}$ for the cross-section approximation 16(b).

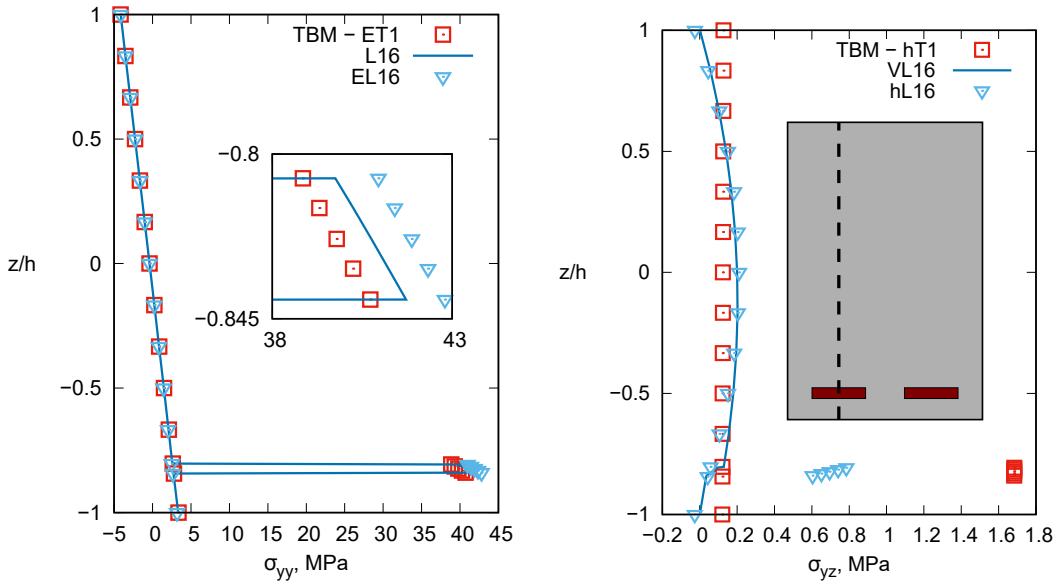

Figure 19: Through-the-thickness σ_{yy} and σ_{yz} distribution for the single RC beam at $y = \dfrac{L}{2}$ for the cross-section approximation 16(b).

Model	$-u_z$, mm at point $(0,\frac{L}{2},0)$	$-\sigma_{yy,c}$, MPa at $\frac{L}{2}$	$\sigma_{yy,s}$, MPa at $\frac{L}{2}$	DOFs
Analytical [39]	3.8216	4.1477	40.4084	-
EBBM	3.8387	4.1545	39.7998	183
CW	3.9207	4.1577	40.4811	206058

Table 4: Values of the transverse displacement of point $(0,\frac{L}{2},0)$ and axial concrete and steel stress of a simply supported RC beam undergoing a vertical uniform pressure. Analytical solution compared to the homogenized and CW models of Fig. 16(c).

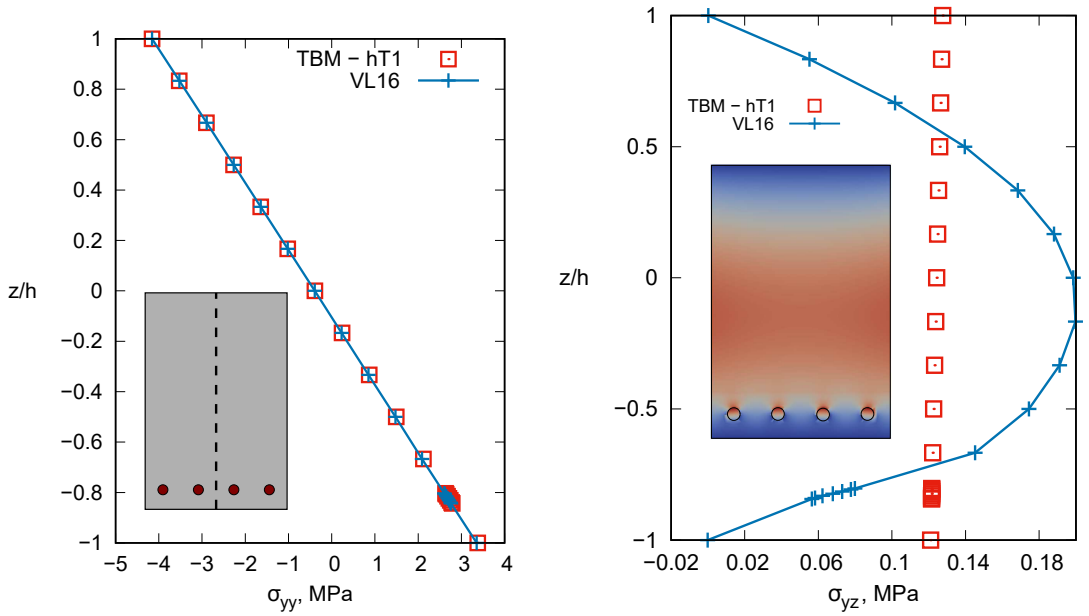

Figure 20: Through-the-thickness σ_{yy} and σ_{yz} distribution for the single RC beam at $y = \dfrac{L}{2}$ for the cross-section approximation 16(c).

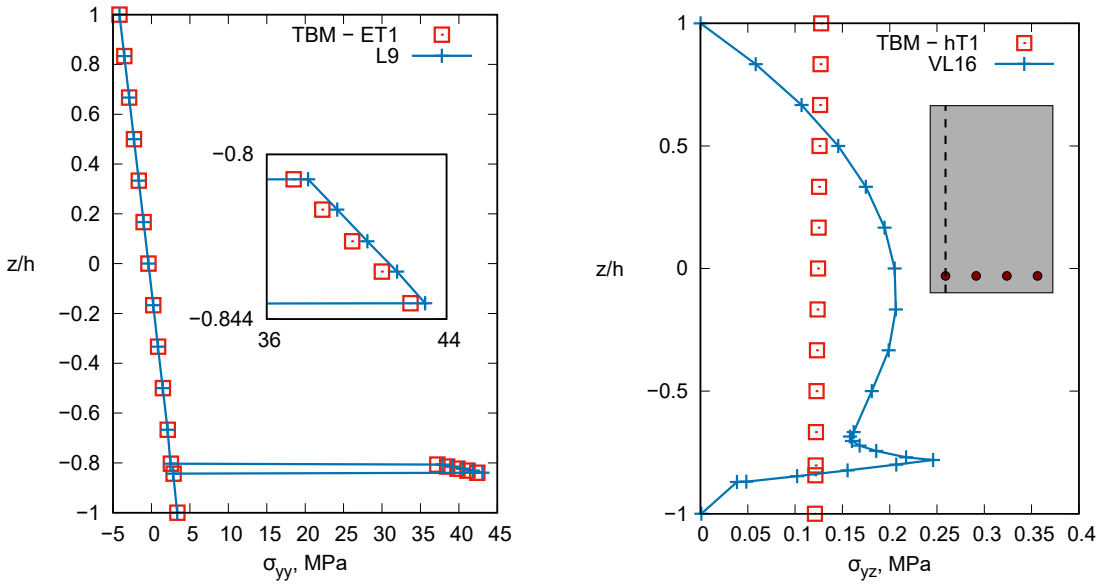

Figure 21: Through-the-thickness σ_{yz} and σ_{yz} distribution for the single RC beam at $y = \dfrac{L}{2}$ for the cross-section approximation 16(c).

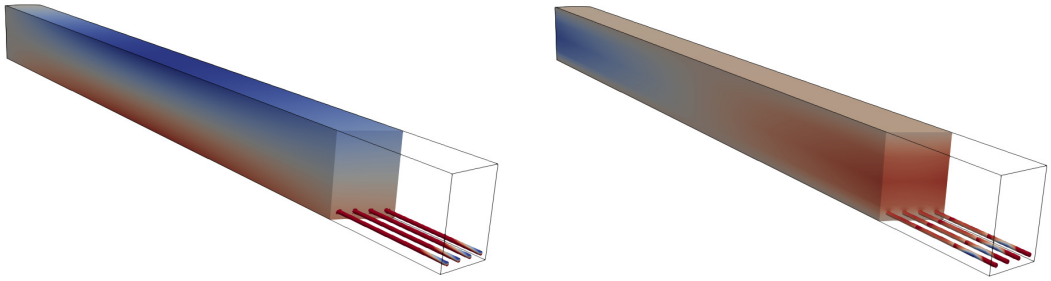

Figure 22: σ_{yz} and σ_{yz} distribution for the single RC beam at $y = \dfrac{L}{2}$ for the cross-section approximation 16(c).

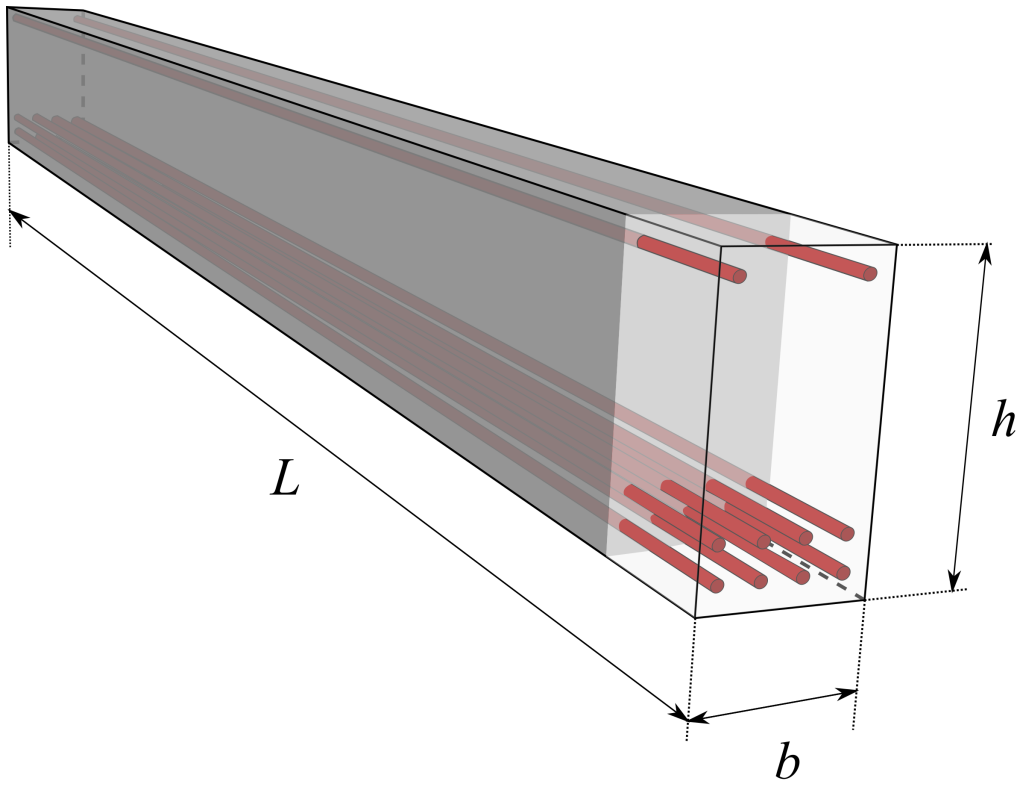

Figure 23: Geometry of the double RC beam.

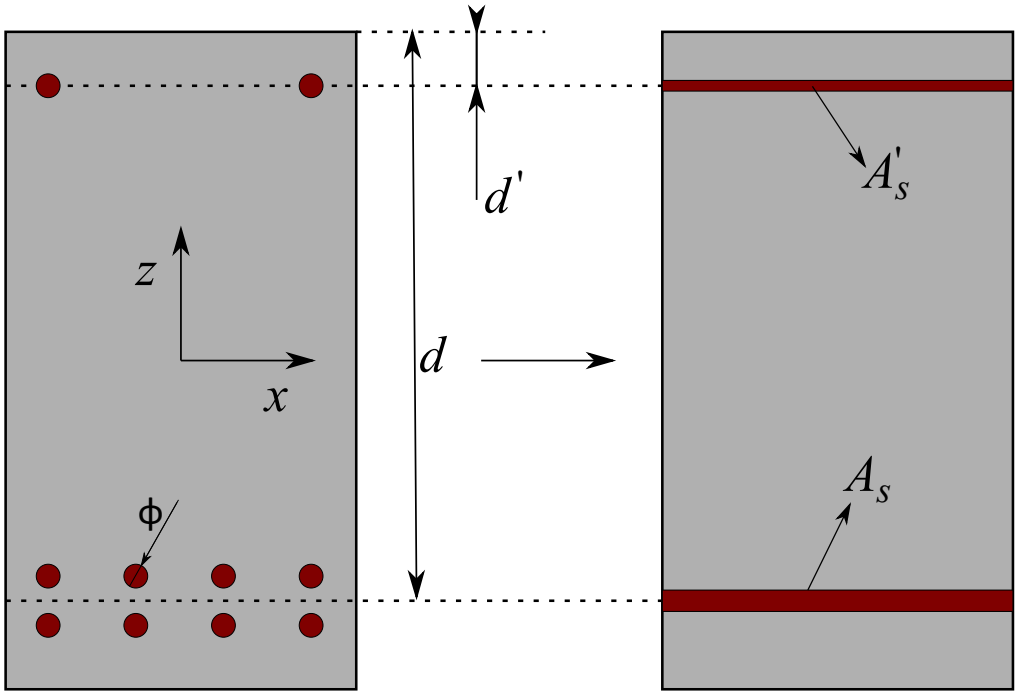

Figure 24: Cross-section geometry of the double RC beam (left) and the current cross-section (rigth).

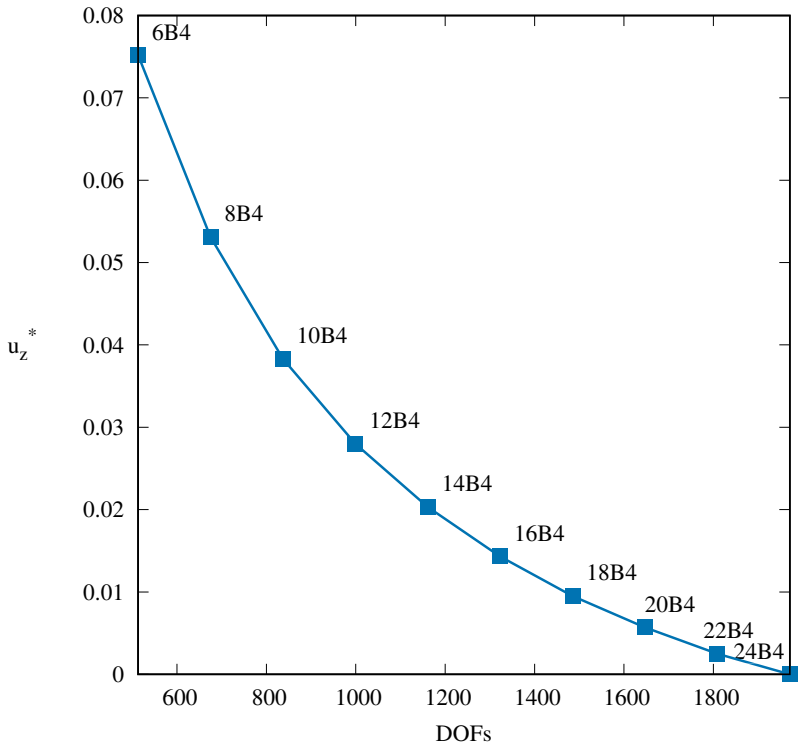

Figure 25: Convergence results for the double RC beam.

beam is simply supported at its ends and subjected to a uniform transverse pressure equals 0.05 MPa. The results are reported in Table 5 in terms of transverse displacement, axial concrete and steel stress, in both compression and tension zones. A good agreement with respect of the analytical results is demonstrated, and the values increas as the refinement of the adopted theory increases. Classical, ESL and LW approaches are employed.

Model	$-u_z \times 10^{-2}$, mm at point $(0,\frac{L}{2},0)$	$-\sigma_{yy,c}$, MPa	$\sigma_{yy,s}$, MPa at $\frac{L}{2}$	$-\sigma'_{yy,s}$, MPa	DOFs
Analytical [39]	4.6270	3.5437	30.9993	45.0633	-
EBBM	4.6302	3.5421	30.6192	45.5356	183
TBM	4.7127	3.5370	30.5127	45.5668	305
hT1	4.7127	3.5370	30.5127	45.5668	549
hT5	4.6681	3.4523	32.3095	48.4454	1098
hT10	4.6975	3.4687	32.2931	48.5222	1830
hL4	4.3773	3.4162	33.0356	50.1058	732
hL9	4.6817	3.4540	32.3071	48.4719	1647
hL16	4.7188	3.4683	32.2930	48.5165	2928
VL4	4.6789	3.5076	30.7426	45.0040	2196
VL9	4.7597	3.5328	31.2629	45.9101	6039
VL16	4.7654	3.5257	31.2934	45.9332	11712

Table 5: Values of the transverse displacement of point $(0,\frac{L}{2},0)$ of a simply supported RC beam undergoing a vertical loading of 100 N. Analytical solution compared to the homogenized and VL models of Fig. 24.

The through-the-thickness distribution of the axial stress is reported in Figs. 26 and 27 for every adopted theory. Similar distribution as the previous example are evaluated and the distribution of the σ_{yy} is accurately evaluated for the concrete and steel materials. The distribution of the shear stress component is reported in Fig. 28. Clearly, classical theories fail on adequately describing the distribution of σ_{yz} in correspondence of the conrete-steel interfaces and over the steel portions, overestimating the stress.
Finally, an application of the ESL approach is adopted hereafter. Three different cross-sectional theories are applied, and they are reported in Fig. 29. Figure 29(a) involves a EL16 element including the compressed steel area, while imposing LPs on both top and bottom interfaces of the tensile steel area. The theories shown in Figs. 29(b, c) employ LPs only on the top and bottom interfaces of the tensile steel area, respectively. The goal of this investigation is to test if the models described in Fig. 29 can be reliable if **only** the σ_{yz} values at both top and bottom interfaces (Fig. 29(a)) or just top/bottom (Fig. 29(b/c)) are wanted, neglecting the accuracy on the compression zone. The results are compared with the L16 theory, here taken as reference.
The results are reported in Table 6. Several conclusions can be drawn:

- The ESL model Fig. 29(a) reports the same σ_{yz} values at both top and bottom interfaces compared to the L16 model, provig that the tensile steel zone can be neglected with this approach.

- If one is interested only on the top of bottom interface, it is enough to impose LPs on the correspondent interface. In fact, the model shown in Fig. 29(b)can adequately

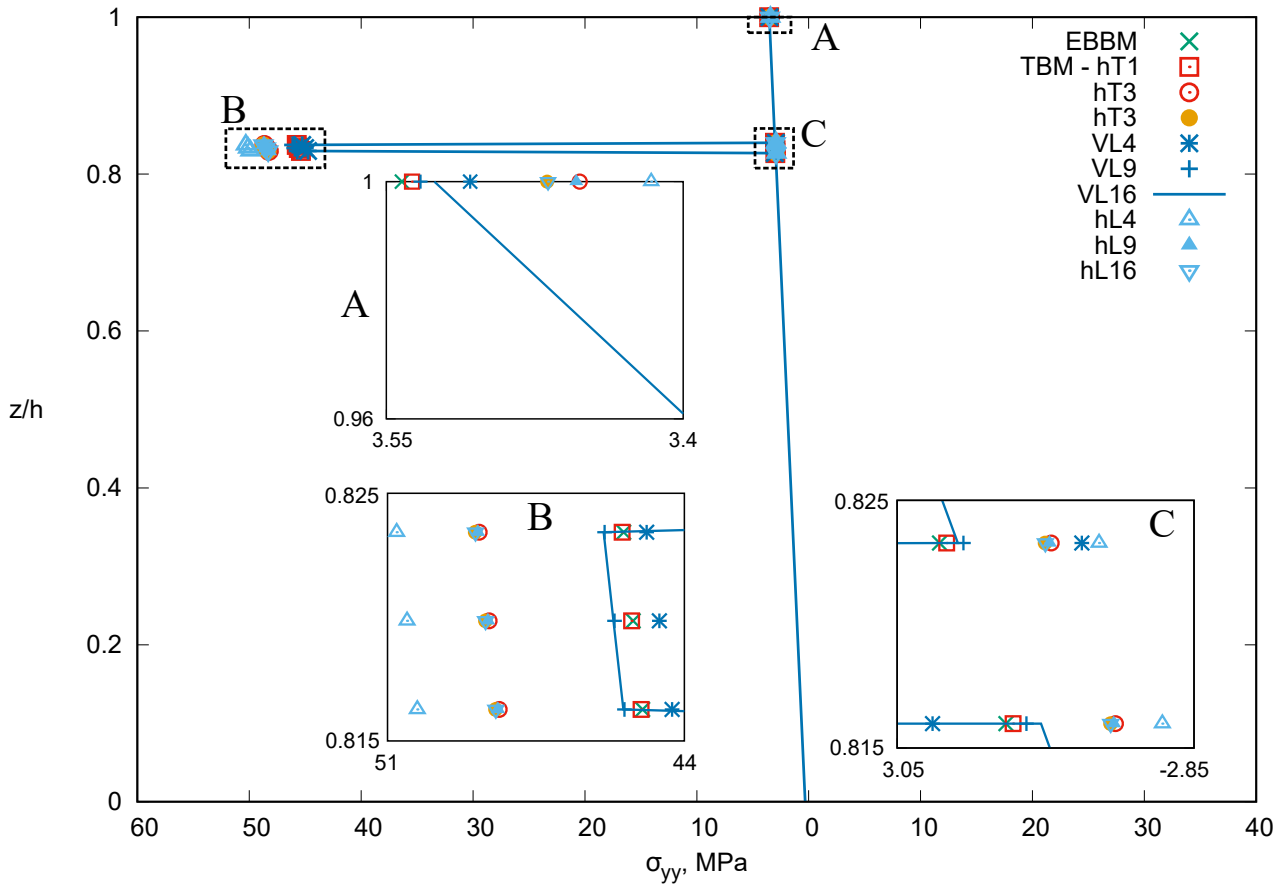

Figure 26: Through-the-thickness σ_{yy} distribution for the double RC beam at $y = \dfrac{L}{2}$.

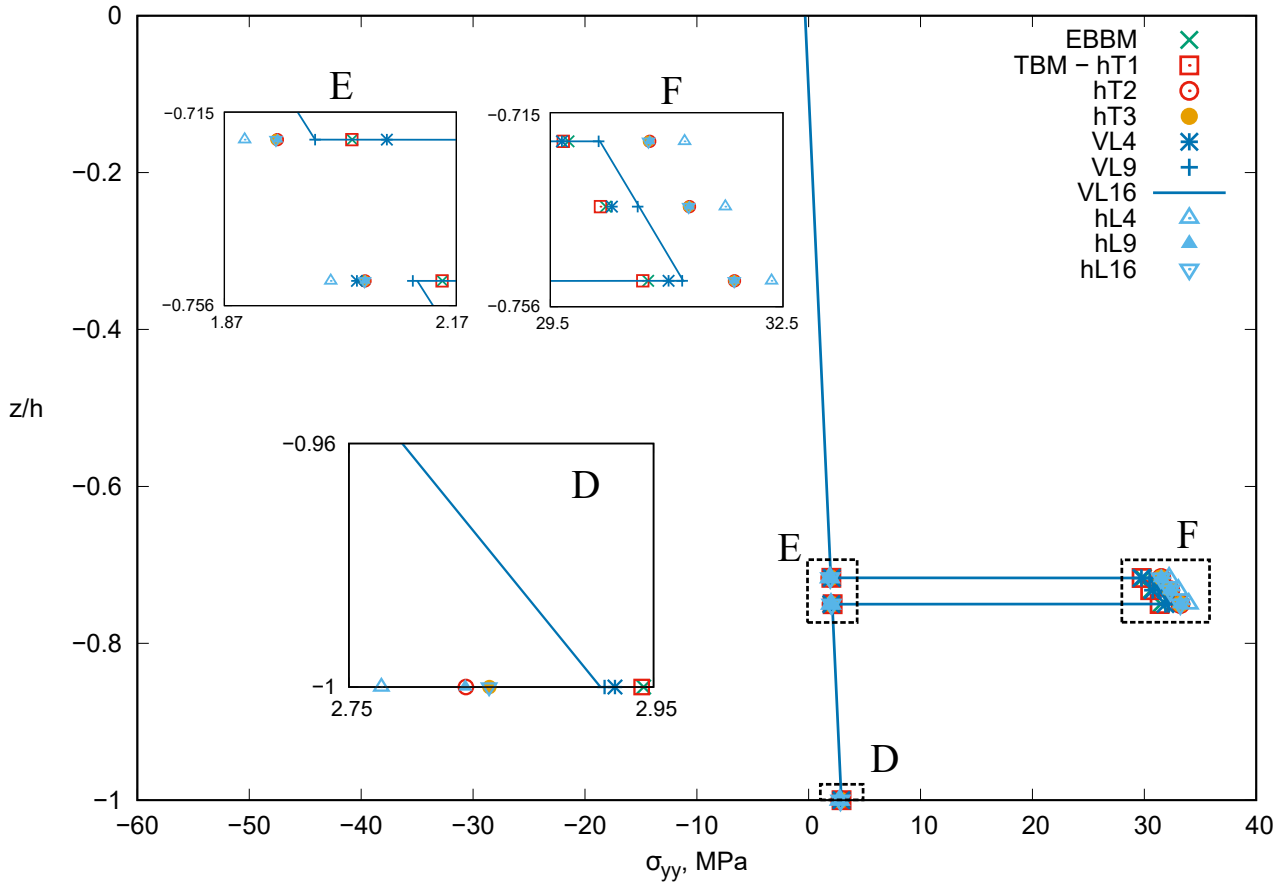

Figure 27: Through-the-thickness σ_{yy} distribution for the double RC beam at $y = \dfrac{L}{2}$.

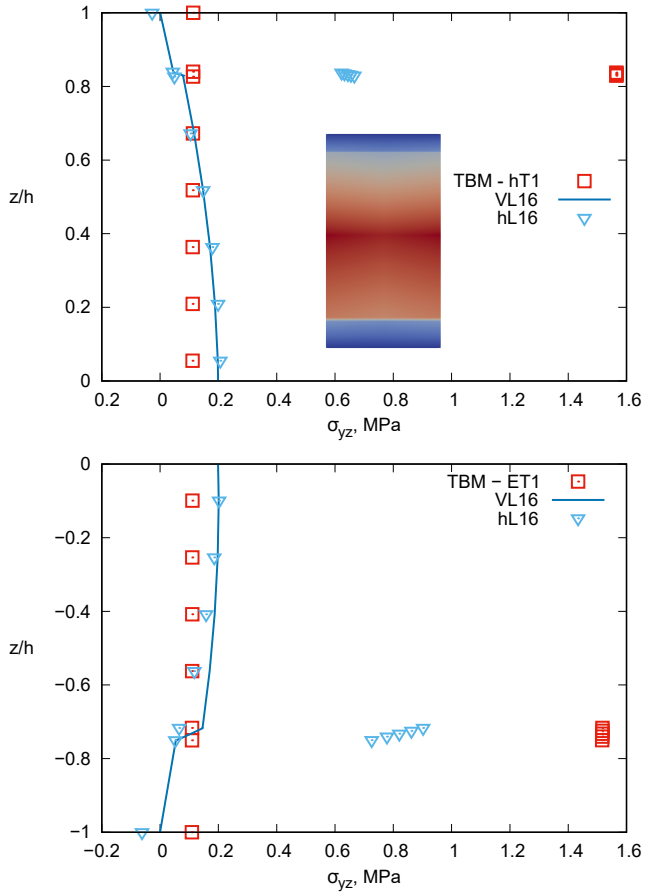

Figure 28: Through-the-thickness σ_{yz} distribution for the double RC beam at $y = \dfrac{3L}{4}$.

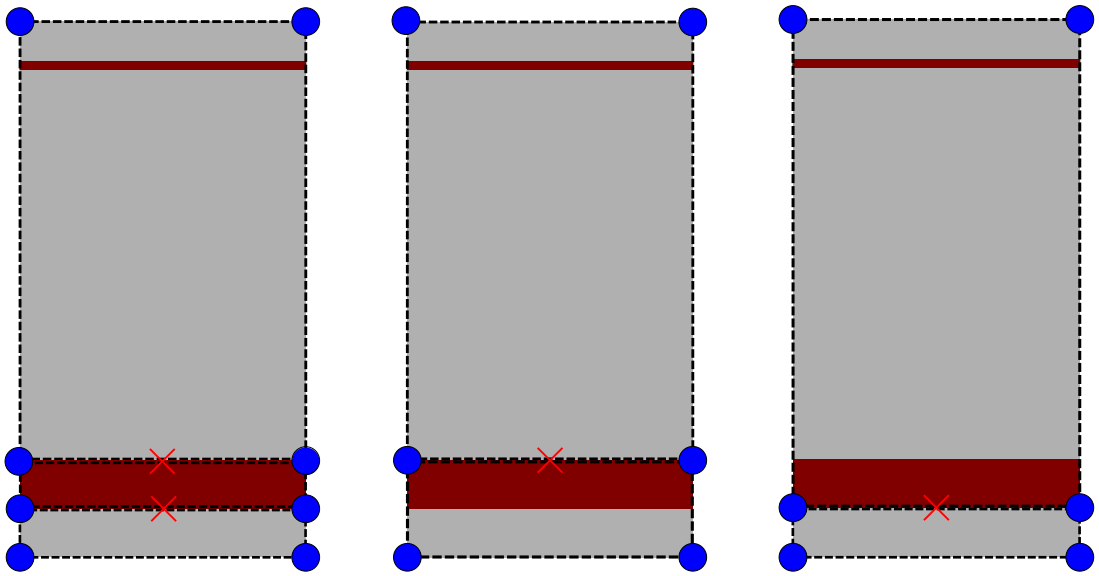

(a) (b) (c)

Figure 29: Schematic rapresentation of three different double RC corss-section approximations. LP on both top and bottom sides of the steel (a), LP on top side of the steel (b) and LP on bottom side of the steel (c).

evaluate the top interface, while failing on describing the bottom one and viceversa for the model shown in Fig. 29(c)

Model	$-\sigma_{yz,TOP}$, MPa	$-\sigma_{yz,BOTTOM}$, MPa	DOFs
VL16	0.1457	0.0540	11712
Fig. 29(a)	0.1446	0.0539	7320
Fig. 29(b)	0.1446	0.0169	5124
Fig. 29(c)	0.0489	0.0532	5214

Table 6: Values of the shear stress component for different double RC cross-section approximation (see Fig. 29). $\sigma_{yz,TOP}$ and $\sigma_{yz,BOTTOM}$ are evaluated in correspondence of the red crosses.

Finally, the through-the-thickness σ_{yz} distribution is reported in Fig. 30. It can be state that the present model allows the user to choose which side of the interface to analyse, gaining DOFs and, consequently, computational cost, without any loss of accuracy.

4.3 Single RC slab

The third study case regards a single RC slab, as shown in Fig. 31(a). The adopted approach is to analyze representative portion of the structus, which results to be a T-shape beam. The geometry of it is taken by [39] and it is reported in Fig. 31(b). where L = 8130 mm, b = 813 mm, b_w = 203 mm, d = 305 mm, D = 339 mm, h_f = 102 mm, and A_s = 1935 mm^2.
The employed mathematical model is reported in Fig. 32, and 20 B4 Fes (in blue) are adopted for the beam axis discretization, along with 6 LE for the cross-section LW approximation. Table 7 reports the values of the midspan deflection and axial concrete and steel stresses. The results show a great accuracy between the adopted theories and the analytical results, being the L16 approach the closest to them, in particular for the axial steel stress.

Model	$-u_z$, mm at point $(0,\frac{L}{2},0)$	$-\sigma_{yy,c}$, MPa at $\frac{L}{2}$	$\sigma_{yy,s}$, MPa at $\frac{L}{2}$	DOFs
Analytical [39]	56.4832	16.7751	273.8205	-
EBBM	54.9673	16.2612	268.5704	183
TBM	55.1949	16.2385	268.1975	305
VL16	55.2803	16.2071	274.0356	13908

Table 7: Values of the transverse displacement of point $(0,\frac{L}{2},0)$ and axial concrete and steel stress of a T-shape single RC beam.

Finally, the through-the-thickness distribution of the axial and shear stresses at $y = \frac{L}{2}$ and $y = \frac{3L}{4}$, respectively.

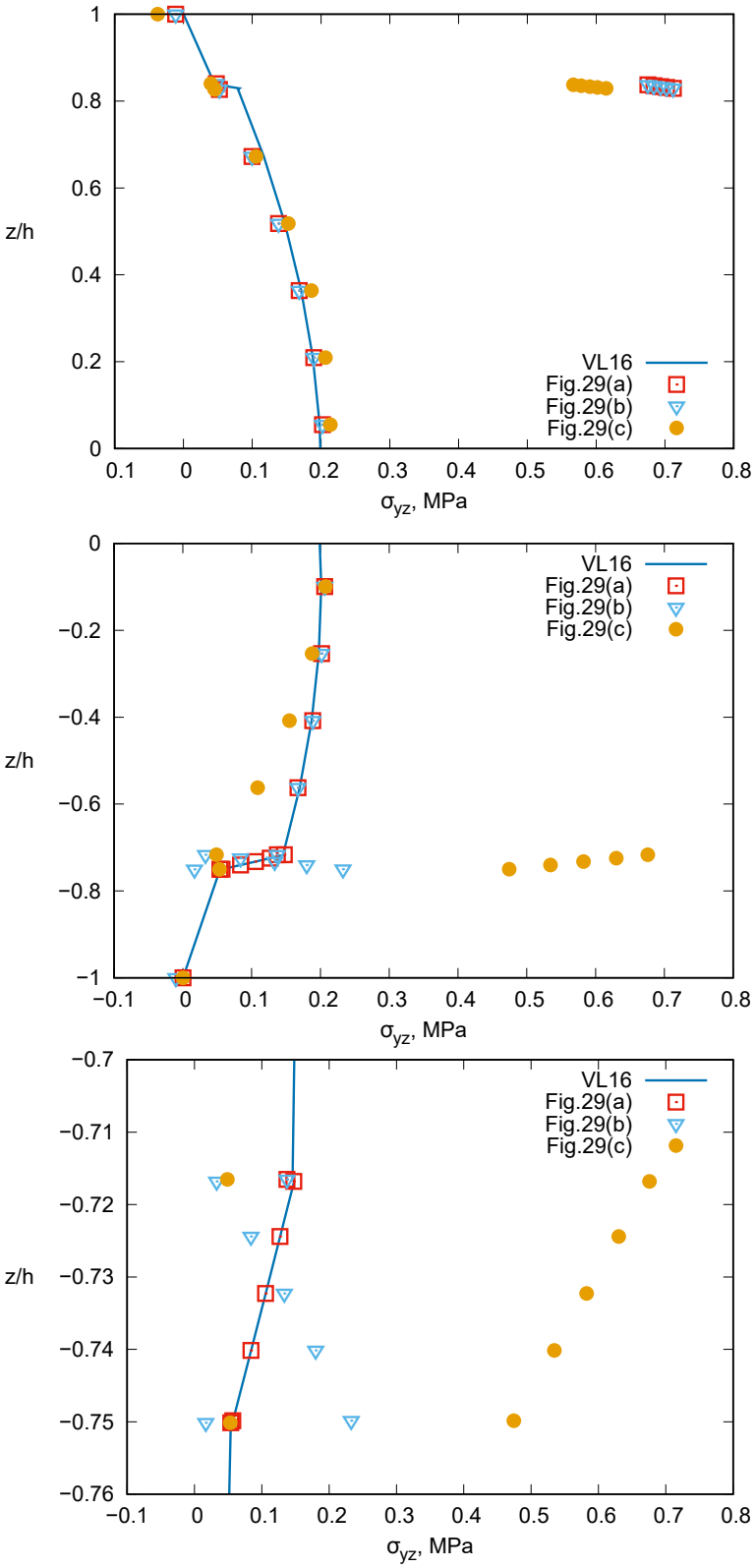

Figure 30: Through-the-thickness σ_{yz} distribution for the double RC beam at $y = \dfrac{L}{2}$, adopting the cross-section approximations shown in Fig. 29.

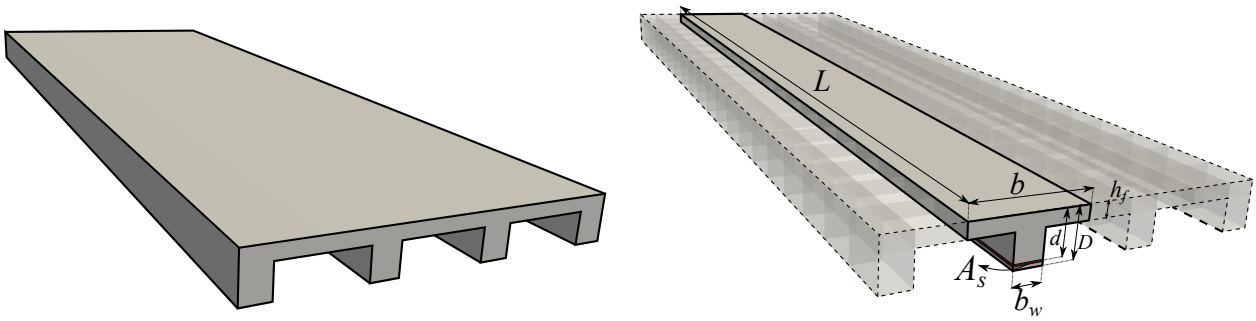

(a) (b)

Figure 31: Geometry of the single RC slab (a) and particular on the analyzed T beam (b).

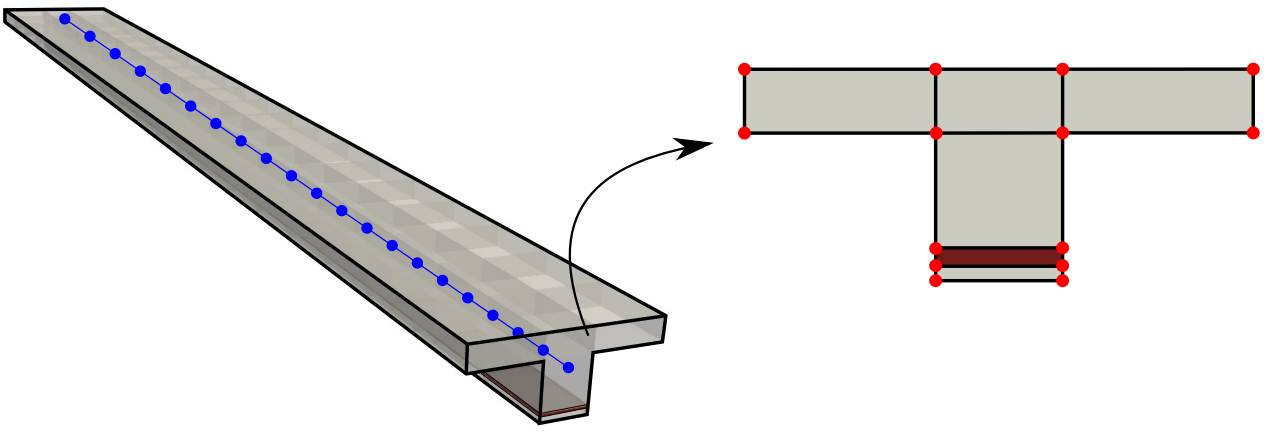

Figure 32: Axial and cross-sectional mathematical model of the T-shape RC beam.

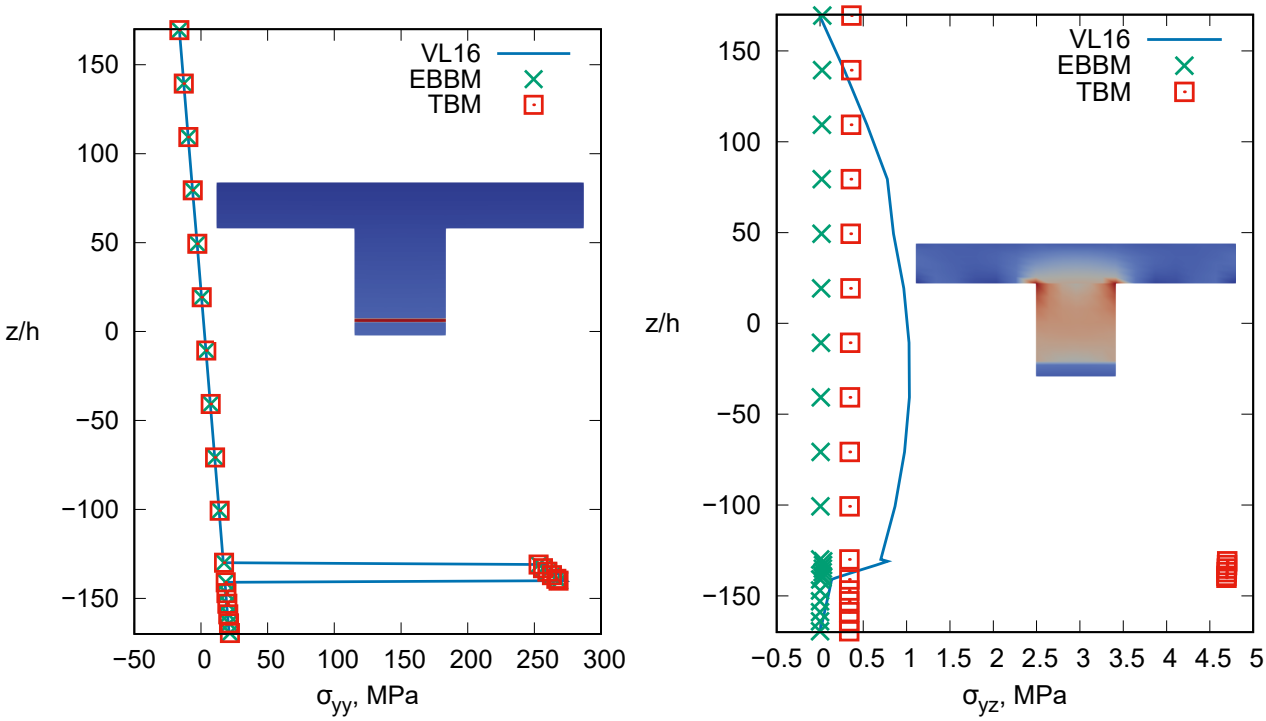

(a) (b)

Figure 33: Through-the-thickness σ_{yy} and σ_{yz} distribution for the T-shape single RC beam at $y = \dfrac{L}{2}$ and $y = \dfrac{3L}{4}$, respectively.

4.4 Double RC beam with stirrups

As a final example, the CW capability of the present approach is further proved on a dobule RC beam with stirrups. The analysis case is taken from the work of Azam *et al.* [45]. The geometric, boundary and loading conditions are reported in Fig. 34, where L = 2700 mm, b = 250 mm, h = 400 mm, s_1 = 250 mm, s_2 = 66,7 mm, a = 200 mm and c = 300 mm. 6 mm stirrups at a spacing of 250 mm c/c are adopted, along with six bars in the tension zone and three in the compression one. Every bar has a diameter of 25.2 mm. One B4 FE are employed for the approximations of the axis between two adjacent stirrups, and one B2 FE for every stirrup, whereas the CW approach is adopted for the cross-sectional approximation and to give a own kinematic for concrete, steel stirrups and reinforcement bars. The total number of DOFS is 129780. The Young modulus of the concrete is set as 14000 Mpa, whereas 200000 MPa for the steel.
Figure 35 reports the numerical simulation of the experimental test reported in the reference work, where the external load over the transverse midsap displacement is reported. Clearly, the present model is able to accurately dercibe the linear behavior of the structure, whereas the nonlinear one is described by the experimental results. The deformed configuration is reported.
Finally, the axial and shear component of the stress are reported in Fig. 36.

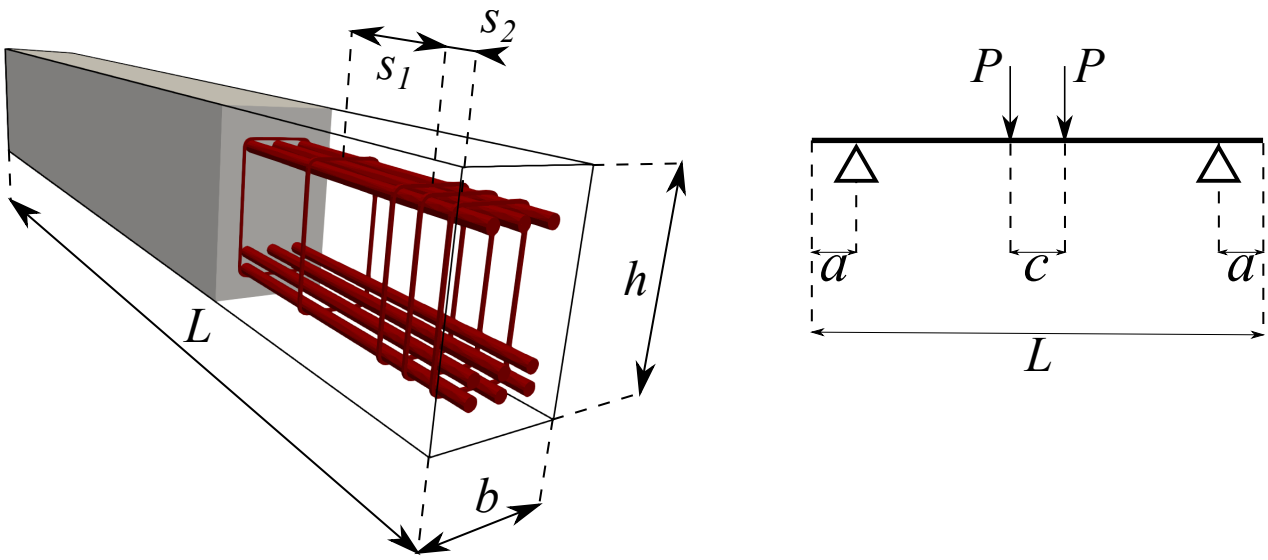

(a)

Figure 34: Geometry of the double RC beam with stirrups.

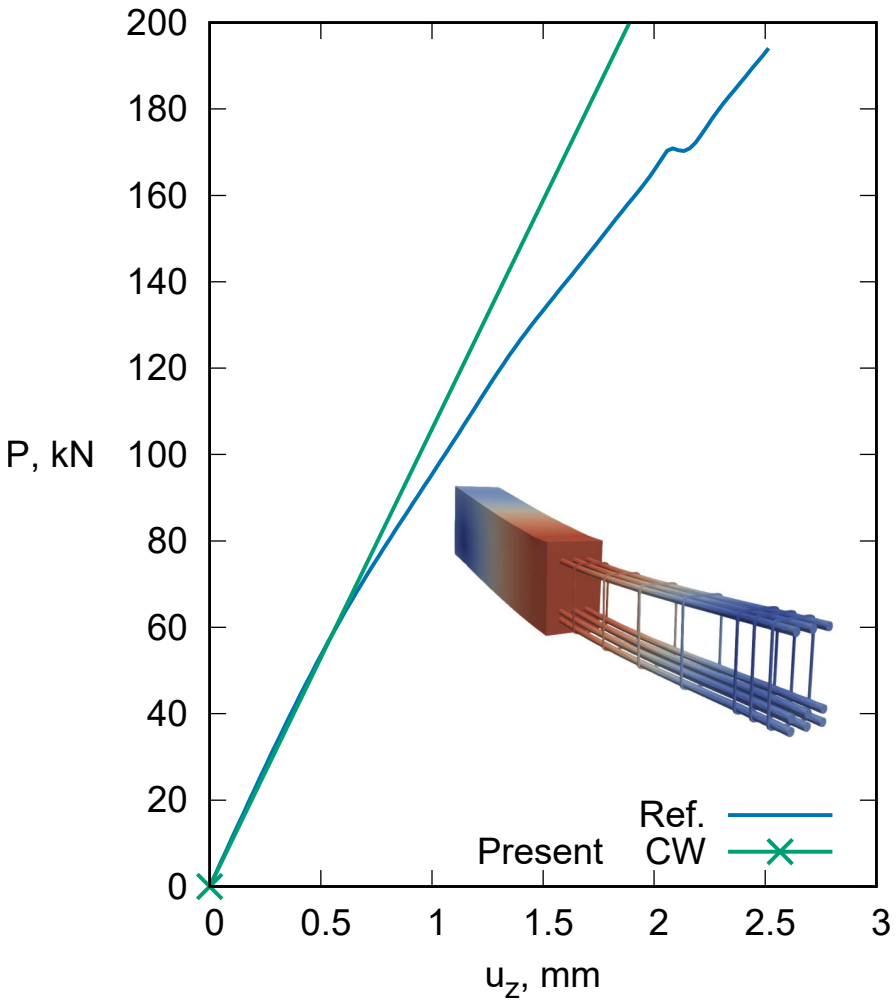

Figure 35: Displacement of the double RC beam with stirrups. reference solution from [45].

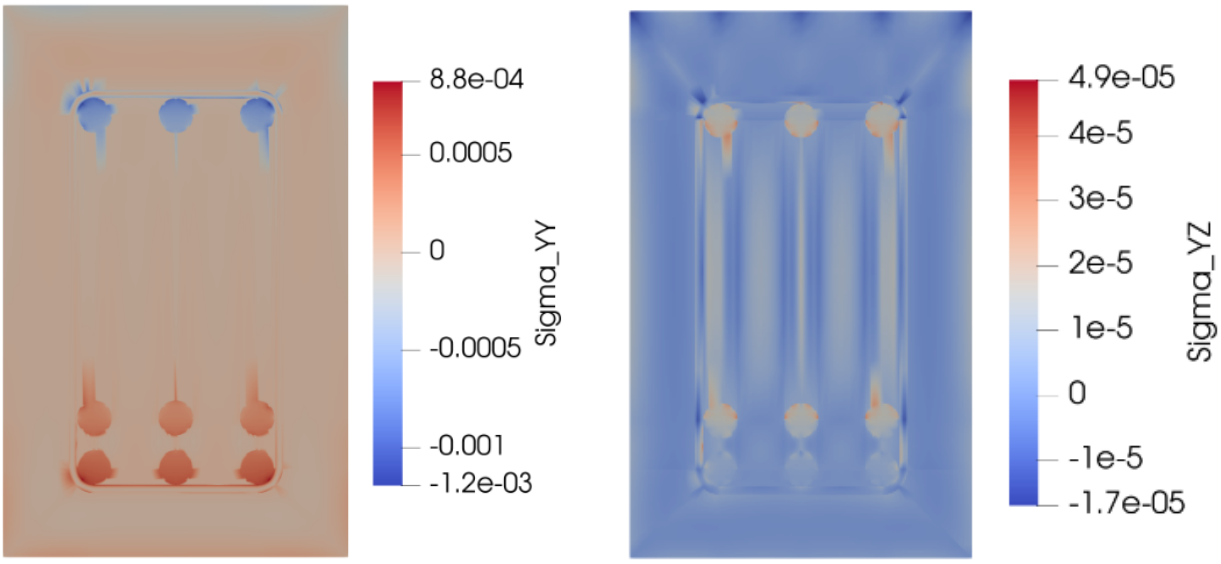

Figure 36: Through-the-thickness σ_{yy} and σ_{yz} distribution for the double RC beam with stirrups at $y = \dfrac{L}{2}$.

5 Conclusions

The present research work was addressed to enstablish a unified one-dimensional (1D) formulation for the structural analysis of Reinforec Concrete (RC) components. The Finite Elements (FEs) are employed in the framework of the Carrera Unified Formulation (CUF), and particular attention is given to various modeling approaches for the cross-sectional discretization. In particular, the heterogeneous mechanical properties of the steel and concrete can be homogenized into a uniform cross-section or a Virtual Layer (VL) can be built to transform the steel rounds into a layer, as happens in composite structures. Finally, the Component-Wise (CW) approach is adoped to analyze indipendently the steel and concrete domains, by the usage of Lagrange Elements (LE). Both single and double RC structure are analyzed, and the modeling approaches turned to be reliable in terms of displacement and and axial stress, by comparing their solution with analytical ones. However, when dealing with shear stress component, the adoption of the CW approach is demanded, to accurately describe the stress situation in the interface between concrete and steel. In addition, a single RC T-shape beam is investigated and the results are evaluated using the aforementioned modeling approaches. Finally, a RC beam with stirrups is studied and the result are compared with experimental ones. A great match between the numerical simulation and experimental tests is achieved, until the plasticity occurs in the concrete/steel interface. Future works will include a node-dependent kinematic approach to the model (see [46]) to cut down the number of degrees of freedom for the mathematical model. Moreover, the Willam and Warnke [47] failure criterion will be considered to model the mechanical behavior of concrete and steel rebars.

References

[1] H. Takizawa. Notes on some basic problems in inelastic analysis of planar R/C structures. *Transactions of the Architectural Institute of Japan*, 240:51–62, 1976.

[2] H. Umemura and H. Takizawa. *Dynamic response of reinforced concrete buildings*, volume 2. Iabse, 1982.

[3] L. Euler. De curvis elasticis, 1944. *Bousquet, Geneva*.

[4] W. A. Oldfather, C. A. Ellis, and D. M. Brown. Leonhard euler's elastic curves. *Isis*, 20(1):72–160, 1933.

[5] S. P. Timoshenko. On the correction for shear of the differential equation for transverse vibrations of prizmatic bars. *Phil Mag.*, 41(245):744–746, 1922.

[6] S. P. Timoshenko. On the transverse vibrations of bars of uniform cross-section. *The London, Edinburgh, and Dublin Philosophical Magazine and Journal of Science*, 43(253):125–131, 1922.

[7] V. V. Novozhilov. *Theory of Elasticity*. Pergamon Press, New York, 1961.

[8] V. Z. Vlasov. *Thin-walled elastic beams*. National Science Foundation, Washington, DC.

[9] R. K. Kapania and S. Raciti. Recent advances in analysis of laminated beams and plates. part i-sheareffects and buckling. *AIAA journal*, 27(7):923–935, 1989.

[10] R. K. Kapania and S. Raciti. Recent advances in analysis of laminated beams and plates, part ii: Vibrations and wave propagation. *AIAA journal*, 27(7):935–946, 1989.

[11] R. El Fatmi and H. Zenzri. On the structural behavior and the Saint-Venant solution in the exact beam theory: application to laminated composite beams. *Computers & structures*, 80(16-17):1441–1456, 2002.

[12] R. El Fatmi. Non-uniform warping including the effects of torsion and shear forces. part i: A general beam theory. *International Journal of Solids and Structures*, 44(18-19):5912–5929, 2007.

[13] R. El Fatmi. Non-uniform warping including the effects of torsion and shear forces. part ii: Analytical and numerical applications. *International Journal of Solids and Structures*, 44(18-19):5930–5952, 2007.

[14] P. Ladevèze and J. Simmonds. New concepts for linear beam theory with arbitrary geometry and loading. *European Journal of Mechanics-A/Solids*, 17(3):377–402, 1998.

[15] P. Ladéveze, P. H. Sanchez, and J. G. Simmonds. Beamlike (Saint-Venant) solutions for fully anisotropic elastic tubes of arbitrary closed cross section. *International Journal of Solids and Structures*, 41(7):1925–1944, 2004.

[16] O. Rand. Free vibration of thin-walled composite blades. *Composite structures*, 28(2):169–180, 1994.

[17] C. Kim and S. R. White. Thick-walled composite beam theory including 3-d elastic effects and torsional warping. *International journal of solids and Structures*, 34(31-32):4237–4259, 1997.

[18] V. Berdichevsky, E. Armanios, and A. Badir. Theory of anisotropic thin-walled closed-cross-section beams. *Composites Engineering*, 2(5-7):411–432, 1992.

[19] V. V. Volovoi, D. H. Hodges, V. L. Berdichevsky, and V. G. Sutyrin. Asymptotic theory for static behavior of elastic anisotropic i-beams. *International Journal of Solids and Structures*, 36(7):1017–1043, 1999.

[20] B. Popescu and D. H. Hodges. On asymptotically correct timoshenko-like anisotropic beam theory. *International Journal of Solids and Structures*, 37(3):535–558, 2000.

[21] W. Yu, V. V. Volovoi, D. H. Hodges, and X. Hong. Validation of the variational asymptotic beam sectional analysis. *AIAA journal*, 40(10):2105–2112, 2002.

[22] W. Yu and D. H. Hodges. Elasticity solutions versus asymptotic sectional analysis of homogeneous, isotropic, prismatic beams. *J. Appl. Mech.*, 71(1):15–23, 2004.

[23] W. Yu and D. H. Hodges. Generalized timoshenko theory of the variational asymptotic beam sectional analysis. *Journal of the American Helicopter Society*, 50(1):46–55, 2005.

[24] J.-S. Kim and K. W. Wang. Vibration analysis of composite beams with end effects via the formal asymptotic method. *Journal of Vibration and Acoustics*, 132(4), 2010.

[25] R. D. Firouz-Abadi, H. Haddadpour, and A. B. Novinzadeh. An asymptotic solution to transverse free vibrations of variable-section beams. *Journal of sound and vibration*, 304(3-5):530–540, 2007.

[26] R. Schardt. Eine erweiterung der technischen biegetheorie zur berechnung prismatischer faltwerke. der stahlbau 35 (1966), pp. 161–171.

[27] N. Silvestre and D. Camotim. First-order generalised beam theory for arbitrary orthotropic materials. *Thin-Walled Structures*, 40(9):755–789, 2002.

[28] N. Silvestre. Generalised beam theory to analyse the buckling behaviour of circular cylindrical shells and tubes. *Thin-Walled Structures*, 45(2):185–198, 2007.

[29] R. Bebiano, N. Silvestre, and D. Camotim. Local and global vibration of thin-walled members subjected to compression and non-uniform bending. *Journal of Sound and Vibration*, 315(3):509–535, 2008.

[30] K. Washizu. Variational methos in elasticity and plasticity. *International Series of Monographs in Aeronautics and Astronautics*, 1968.

[31] E. Carrera, G. Giunta, and M. Petrolo. *Beam structures: classical and advanced theories*. John Wiley & Sons, 2011.

[32] E. Carrera, G. Giunta, P. Nali, and M. Petrolo. Refined beam elements with arbitrary cross-section geometries. *Computers & structures*, 88(5-6):283–293, 2010.

[33] E. Carrera, M. Petrolo, and E. Zappino. Performance of cuf approach to analyze the structural behavior of slender bodies. *Journal of Structural Engineering*, 138(2):285–297, 2012.

[34] E. Carrera, M. Petrolo, and P. Nali. Unified formulation applied to free vibrations finite element analysis of beams with arbitrary section. *Shock and Vibration*, 18(3):485–502, 2011.

[35] A. Pagani, M. Boscolo, J. R. Banerjee, and E. Carrera. Exact dynamic stiffness elements based on one-dimensional higher-order theories for free vibration analysis of solid and thin-walled structures. *Journal of Sound and Vibration*, 332(23):6104–6127, 2013.

[36] E. Carrera, A. Pagani, M. Petrolo, and E. Zappino. A component-wise approach in structural analysis. *Computational methods for engineering science*, 4:75–115, 2012.

[37] E. Carrera, M. Maiarú, and M. Petrolo. Component-wise analysis of laminated anisotropic composites. *International Journal of Solids and Structures*, 49(13):1839–1851, 2012.

[38] E. Carrera and M. Petrolo. Refined one-dimensional formulations for laminated structure analysis. *AIAA journal*, 50(1):176–189, 2012.

[39] R. Park and T. Paulay. *Reinforced concrete structures*. John Wiley & Sons, 1975.

[40] E. Carrera, M. Cinefra, M. Petrolo, and E. Zappino. *Finite Element Analysis of Structures through Unified Formulation*. John Wiley & Sons, Chichester, West Sussex, UK., 2014.

[41] E. Carrera. Mixed layer-wise models for multilayered plates analysis. *Composite Structures*, 43(1):57–70, 1998.

[42] I. Kaleel, M. Petrolo, A. M. Waas, and E. Carrera. Micromechanical progressive failure analysis of fiber-reinforced composite using refined beam models. *Journal of Applied Mechanics*, 85(2), 2018.

[43] K. J. Bathe. *Finite Element Procedure*. Prentice hall, Upper Saddle River, New Jersey, USA, 1996.

[44] E. Carrera, G. Giunta, and M. Petrolo. *Beam Structures: Classical and Advanced Theories*. John Wiley & Sons, 2011.

[45] R. Azam, K. Soudki, J. S. West, and M. Noël. Strengthening of shear-critical rc beams: Alternatives to externally bonded cfrp sheets. *Construction and Building Materials*, 151:494–503, 2017.

[46] E. Carrera and E. Zappino. One-dimensional finite element formulation with node-dependent kinematics. *Computers & Structures*, 192:114–125, 2017.

[47] K. J. Willam. Constitutive model for the triaxial behaviour of concrete. *Proc. Intl. Assoc. Bridge Structl. Engrs*, 19:1–30, 1975.